Accepted Manuscript

Geoenergy

Numerical modelling of the effects of permeability contrasts on underground hydrogen storage in sandstone reservoirs

Douglas Smith, Andreas Busch, Daniel Arnold & Edward Hough

DOI: https://doi.org/10.1144/geoenergy2023-039

To access the most recent version of this article, please click the DOI URL in the line above. When citing this article please include the above DOI.

This article is part of the Hydrogen as a future energy source collection available at: https://www.lyellcollection.org/topic/collections/hydrogen

Received 13 October 2023
Revised 24 January 2024
Accepted 19 March 2024

Numerical modelling of the effects of permeability contrasts on underground hydrogen storage in sandstone reservoirs

Abbreviated title: Modelling permeability contrasts for UHS

Authors: Douglas Smith[1],[2]*, Andreas Busch[1], Daniel Arnold[1], Edward Hough[2]

[1] Lyell Centre, Heriot-Watt University, Edinburgh EH14 4AS, United Kingdom

[2] British Geological Survey, Nicker Hill, Keyworth, Nottingham NG12 5GG, United Kingdom

*Correspondence (dosmi@bgs.ac.uk)

Abstract

Hydrogen is an energy carrier that can balance the divergent variations in seasonal energy demand and energy supply from renewables. Underground hydrogen storage in porous formations, such as depleted gas sandstone reservoirs or saline aquifers, provides the capacities needed for large-scale, long-duration energy balancing. This paper reports on the fundamental behaviour of hydrogen in a model reservoir setup, involving a two-phase (H_2, water) system and a two well (injector, producer) setup placed at different depths in the reservoir. We specifically focus on the impact of natural heterogeneities, and associated permeability contrasts, on flow and efficacy of hydrogen injection and production. We found that positioning the wells, both injector and producer, at the top of the reservoir facilitates the highest hydrogen production. We also found that permeability contrasts of three to four orders of magnitude significantly affect hydrogen flow; however, factors affecting the pressure gradient also need to be considered. These factors include compartmentalisation, the behaviour of co-existing fluids and the localised pressure gradient created by the hydrogen plume. Our research underlines the need to understand the architecture of the whole reservoir, from seismic to sub-seismic scales, not just the zones surrounding the wells and pathways in-between, as this controls capacity, pressure fluctuations and informs operational management decisions.

Introduction

Underground hydrogen storage (UHS) can provide large-scale energy storage suitable for applications such as industrial processes (including production of ammonia or steel), transportation, reconversion to electricity and domestic heating in some circumstances (IEA, 2023a). Hydrogen can balance energy demand and supply from intermittent renewable energy generators and, as such, many governments have adopted hydrogen as part of their future energy mix (AusGov, 2019; de Coninck et al., 2018; UKGov, 2020a; USGov, 2021; IEA, 2021).

To ensure sufficient capacity and availability of hydrogen, to balance seasonal supply and demand, the gas needs to be stored. Underground storage provides ample capacity, building upon decades of experience from subsurface natural gas storage, a proven technology for supplying methane at scale (Scafidi et al., 2021). Even storing hydrogen gas in the subsurface is not new. Hydrogen is a key constituent of town gas (composed of hydrogen, methane, nitrogen and carbon monoxide) with historical underground reservoirs in Teesside (UK), Texas (US), Beynes (France), Lobodice (Czech Republic) and 7 sites in Germany (Hydrogen TCP-Task 42, 2023). Near-pure (95%) hydrogen has been stored successfully in the subsurface in salt caverns, e.g. Teesside (UK) and Texas (US), but the HYBRIT project will expand UHS options by constructing a lined rock cavern (LRC), a purpose-excavated cavern lined with concrete and steel to ensure that it is gas-tight, with the gas used for major industrial processes (Pei et al., 2020; Hydrogen TCP-Task 42, 2023). However, the volumes of gas that can be stored in salt caverns and LRCs limit the use of hydrogen or require a significant number of repositories to be constructed. For instance, the HYBRIT LRC is expected to store up to 100 GWh and it is estimated that 56 salt caverns will be required to store 8 TWh (Mouli-Castillo et al., 2021; LKAB, 2022). For scale, by 2050 the UK Government predicts that between 250 – 460 TWh of hydrogen will be needed to meet Net Zero targets. In contrast the expectation is that the worldwide demand would be over 13 PWh (UKGov, 2021; IEA, 2023b).

Sandstone reservoirs offer storage volumes that are up to two orders of magnitude larger than the largest salt caverns, and are geographically more widespread (Heinemann et al., 2021; Mouli-Castillo et al., 2021; Aftab et al., 2022). There are two types of sandstone storage,

saline aquifers and depleted hydrocarbon reservoirs. Saline aquifers are less commonly used for gas storage and, as a result, lack geological data, which is both time consuming and expensive to acquire (Tarkowski, 2019). Hydrocarbon reservoirs account for the bulk of global natural gas storage (80% of working volumes in 2019: Cedigaz, 2020), benefitting from lower geological uncertainties and existing infrastructure that can be repurposed for transporting hydrogen (Tarkowski, 2019; Kanaani et al., 2022). The first underground storage site to have 100% hydrogen injected into sandstone, utilising a depleted gas field at Gampern (Austria), recently became operational in April 2023 (RAG, 2023).

However, most of our current knowledge of gas storage in porous reservoirs is limited to methane and carbon dioxide. Hydrogen storage in porous media needs further exploration due to its different physical and chemical properties. Hydrogen is a smaller, more mobile molecule, and we do not fully understand how hydrogen behaves alongside other fluids present in a reservoir, particularly in relation to the heterogeneities within a potential sandstone reservoir. In addition, hydrogen has a lower energy density (energy per unit volume) than natural gas, requiring increased storage to accommodate the same quantity of energy so that the suitability of additional storage may need to be explored (Hashemi et al., 2021). Additional capacity is also necessary due to the requirements of balancing seasonal supply and demand (Gasanzade et al., 2021; Mouli-Castillo et al., 2021).

Further understanding of how hydrogen behaves when it is injected and stored in different media is required, particularly as it migrates through heterogeneous subsurface reservoirs. In this respect, we examine how heterogeneity, specifically contrasting permeabilities, affect the injection, plume development and recovery of hydrogen in UHS.

Potential effects of contrasting permeability

Permeability contrasts are created by both sedimentary and structural processes and can either define the reservoir by establishing its boundaries, such as a tight caprock or a sealing fault, or can create barriers or compartments within the reservoir. Sedimentary features can result in architecture of varying complexity and include interbedded (layer-cake), jigsaw or labyrinthine arrangements, and sedimentology can be a strong influence on fluid flow

through such rocks. The more complex arrangements are characterised by adjoining sandstone layers, interspersed with non-continuous, low-permeability strata (Lawrence et al., 2006). Faulting is a structural feature that can have multi-scale impacts, affecting or defining part or the whole reservoir (decimetre to kilometre scale), whereas deformation bands are examples of structures that are more likely to have localised effects (millimetre to decimetre scale) but that still impact upon pressure, plume integrity and gas recoverability (Leveille et al., 1997; Wakefield et al., 2022). Some sedimentary and structural features can be resolved by seismic mapping or be detected from core data. However, many features that create permeability contrasts are below seismic scale and may be abundant within potential porous storage media, such as deformation bands within well-sorted, aeolian facies, or are more extensive than survey data suggests (Leveille et al., 1997; Wakefield et al., 2022).

Compartments can diffuse or trap fluids, affecting pressure and fluid movement and ultimately can reduce the effective storage volume and efficiency of the reservoir. The effects of compartmentalisation have been recognised at both the large, reservoir or aquifer-scale (up to kilometre scale), and at the centimetre, core-scale for water, hydrocarbons and CO_2 but have not been studied in relation to UHS (Leveille et al., 1997; Mohamed and Worden, 2006; Pourmalek et al., 2021). This study provides a gateway into the effect of features created by permeability contrasts at the metre to kilometre-scale.

Utilising Darcy's equation of flow, the low viscosity (μ) of H_2 indicates that the flow rate (u) remains relatively unaffected by pressure gradients (∇P) unless there is a significant change in permeability (k) by several orders of magnitude (Equation 1):

$$u = -\frac{k}{\mu} \nabla (P) \qquad \text{Equation 1}$$

This observation, eponymously called "Flora's rule" by Ringrose and Bentley (2021), predicts three orders of magnitude variation in permeability to observe an impact upon hydrogen flow. We test that prediction using models that quantify the influence of reservoir heterogeneity in a gas-liquid-rock system. We simulate hydrogen storage in an aquifer, as a

depleted hydrocarbon reservoir would also contain gas, adding a further dimension to the simulations, obscuring the outcomes.

Plume integrity, the ability of the gas plume to remain connected, is also potentially affected by heterogeneity. Maintaining a coherent plume is important because more hydrogen can be recovered and less will be lost to processes such as diffusion and dissolution (Amirthan and Perara, 2022). Diffusion and dissolution are not included in this study, to reduce confounding variables when determining the effect of heterogeneity, but viscous fingering, the unequal progression of the injected fluid, is one of the processes being monitored. Viscous fingering leads to the loss of integrity of the plume and is often predicted using the mobility ratio (M) of the two fluids involved. The mobility of each fluid is defined as the effective permeability for that fluid, the product of absolute permeability (k_a) and relative permeability (k_{rH2} for hydrogen and k_{rw} for water), divided by its viscosity (μ_{H2} for hydrogen and μ_w for water). This is used to create a ratio between the fluids, such that (Pan et al., 2021),

$$M = \frac{\left\{\frac{k_a k_{rH2}}{\mu_{H2}}\right\}}{\left\{\frac{k_a k_{rw}}{\mu_w}\right\}} = \frac{k_{rH2}\mu_w}{k_{rw}\mu_{H2}} \quad \text{Equation 2}$$

Viscous fingering is therefore a function of both the fluid and rock properties. The former establishes that fingering is more likely to occur in two phase systems when there is a large viscosity difference between the fluids, such as hydrogen and water. The rock properties control the fluid interaction by modifying contrasting permeabilities, which in turn influence the relative permeabilities of the fluids. There are only two experimental studies that have observed hydrogen flow in a two-phase system with sandstone rock that includes a permeability contrast (Boon and Hajibeygi, 2022; Jangda et al., 2023). Boon and Hajibeygi (2022) describe their layered sample in terms of its porosity and did not make specific findings about the effect of the low porosity on fluid flow; they measured relative permeability across the aggregate of the layers, although the water saturation images across the core during drainage and imbibition highlight some of the effects of low permeability. Jangda et al. (2023) found that preferential pathways are established through low permeability layers and that those layers can reduce storage capacity.

Permeability contrasts are integral to a number of UHS modelling studies, due to the reservoir architecture, particularly in feasibility studies or studies utilising studied rock formations (for instance, Pfeiffer et al., 2017; Lubon and Tarkowski, 2020; Lysyy et al., 2023). However, studies that systematically altered permeability contrasts to observe their impact upon hydrogen production are limited (Arekhov et al., 2023). Here, they undertook a sensitivity analysis of permeability contrasts to determine their effect upon diffusion within UHS. They found that diffusion increases with an increase in permeability contrasts.

We examine the effect of permeability contrasts in the context of UHS at the metre to kilometre scale to determine their effect on flow, plume development and hydrogen injection and recovery. This, in turn, will provide an insight into the reservoir architecture that impacts upon the efficacy of UHS and prescribe what information is pertinent when assessing potential reservoirs. It is our aim to determine the fundamental behaviours of hydrogen in a two-phase system in relation to permeability contrasts so that the findings can be applied to a range of UHS scenarios.

Method

Modelling concept

In this study, we use different combinations of well placements in a series of layered geological models with increasing permeability contrasts with the aim of understanding the effect of heterogeneity in a two-phase (hydrogen-water) reservoir. In addition to observing the fluid pathways, we quantify the effect of permeability contrasts using hydrogen and water production forecasts, average reservoir pressure and bottom-hole pressure (BHP). We particularly study how heterogeneity affects plume integrity and structural trapping, which both impact upon reservoir effectiveness (Aftab et al., 2022). We use the Computer Modelling Group (CMG) reservoir simulator (version 2021.10) to build the reservoir models and the GEM software to run the fluid flow simulations. The Peng-Robinson (Robinson, 1978) equation of state is used to calculate the relationship between the fluids.

Our aim is to conduct generic, non-site-specific research, so that the findings can be applied to understand the behaviour of hydrogen in different UHS settings. Although we use an analogue for porosity and permeability data for our geological models, our study is not intended to investigate the analogue formation's suitability for UHS and does not include a detailed analysis of its geology. The analogue we use is from the Jurassic Navajo sandstone at Green River, Utah, used previously for studying natural CO_2 accumulations (Kampman et al, 2014). **Figure 1** shows the stratigraphy, porosity and permeability data of the Navajo sandstone from a borehole drilled near Crystal Geyser. The geological models replicate the thickness of the Navajo sandstone unit (85 m), although a hydrodynamically connected layer has been added at the base to simulate aquifer support (a further 10 m but the volume has been artificially increased). There are no-flow boundaries in all other directions. The plan-view area (2.25 km^2) and the depth at which they are situated (1000 m at the top of the reservoir) were chosen to be similar to other hydrogen reservoir models to give them comparable representative reservoir properties such as temperature, pressure and capacity (Feldmann et al., 2016; Mahdi et al., 2021). In this study, the term 'reservoir' refers to the four zones, simulated from the properties of Navajo sandstone, above the aquifer-like zone. The approximate location of the zones, based upon the permeability properties and facies type of the Navajo sandstone, are shown in **Figure 1**.

The vertical heterogeneity of the models is increased by inserting a low permeability zone (LPZ) at one of two depths, in between zones 1 and 2 or zones 2 and 3, to maximise the permeability contrasts observed. The permeability range of the LPZs (10 mD – 10^{-5} mD) covers permeability from one order of magnitude below the highest permeability in the models to that of tight rocks like mudstones (Ringrose and Bentley, 2021). The range also enables the Flora's rule prediction (see above) to be tested as the lowest permeability is 4 orders of magnitude below the permeabilities of the least permeable layers in the basic models (0.24 and 0.32 mD); one order of magnitude more than the prediction. Although the lateral and continuous properties and uniformity of the LPZs are exaggerated they force the reservoir fluids to interact with the permeability contrasts. This enables us to observe and understand the effects of those contrasts.

In relation to the dynamic modelling, we use a universal Brooks-Corey, relative permeability relationship (described further below), as in the studies conducted by Pfeiffer et al. (2016), Lubon and Tarkowski (2020), Mahdi et al. (2021) and Chai et al. (2023), where they used either the Corey-type or Van Genuchten–Mualem relationships in their models. We also used a single drainage relative permeability relationship for both drainage and imbibition, so our results do not take account of effects that arise when different relative permeability relationships are used for the two processes (Lysyy et al., 2023). After preliminary analysis we have not included capillary pressure data within our models as their effects on the simulation outputs were small, particularly in high permeability reservoirs, and other studies look at this phenomenon in more detail (for instance, see Wang et al. (2022) for the effects of capillary pressure on fluid flow and recovery factor).

Our flow simulations focus on addressing the impact of vertical permeability contrasts at the metre to kilometre scale on effective cyclical hydrogen storage for a single, central injection or production well, rather than optimising reservoir performance in terms of well count, injection or production pressures, and hydrogen or water production. Therefore, we do not use pre-operational cushion gas as it would mask the effects of the permeability contrasts on hydrogen distribution in our geological models. As a result, we permit conditions which would otherwise be unrealistic and uneconomic, such as allowing the BHP to increase to 1000 MPa

during injection or reduce to atmospheric pressure during production. The former parameter, in relation to injection, enable the same amount of hydrogen to be injected into each reservoir simulation, so that simulation outputs can be directly compared. The latter limit allows the effects of the fluid flow in relation to the permeability contrasts to be observed, otherwise production well shut-in would be almost immediate for a number of scenarios, inhibiting the creation of pathways.

Previous studies have tested various operational strategies from a single three-year injection and one-year production cycle to ten cycles of eight months injection and four months production (Mahdi et al., 2021; Zamehrian and Sedaee, 2022). We chose four cycles, the first three mimic seasonal supply and demand and have an eight-month injection to four-month production period ratio. This provides sufficient time for the hydrogen to migrate into the reservoir and view the impact of permeability contrasts between zones. During the first three cycles, more gas is injected than recovered, resulting in an accumulation of gas until the last production period which showcases how heterogeneity within the reservoir can impact the distribution and availability of hydrogen in line with previous studies (Lysyy et al., 2021; Kanaani et al., 2022; Zamehrian and Sedaee., 2022). To observe ultimate hydrogen recoverability, we chose a fixed final production period that prevented any models from maintaining a required production rate throughout the cycle. This consequence may also be observed in previous production cycles if insufficient gas is available to the producer, i.e., if it has been trapped or dispersed beyond the influence of the producer.

Chemical reactions and anaerobic digestion play a crucial role in ensuring the success of hydrogen storage but are not considered in this study. There are detailed discussions on these processes in publications by Pan et al. (2021), Aftab et al. (2022), Muhammed et al. (2022), and Miocic et al. (2023).

Reservoir model

To start we compare a basic heterogeneous model with a basic homogenous model. This comparison will show if there are any observable effects of metre-scale layering when cycling hydrogen through a reservoir. Both models have the same physical dimensions (**Table 1** and

Figure 2) but where the basic homogenous model uses the formation arithmetic average values for porosity (11.64%) and permeability (35mD), the basic heterogeneous reservoir has four layers with thickness, permeability and porosity reflecting those of the four main Navajo zones (**Figure 1** and **Table 2**). We use arithmetic average values for porosity and permeability within each zone of the basic heterogeneous model such that there are strong contrasts between zones, creating an array of vertical permeability contrasts but no grid-scale heterogeneity within each zone (**Table 2**).

Both models have no-flow, Neumann-type boundaries on all sides and at the top of the reservoir, to represent a reservoir compartment with sealing faults and a low permeability caprock. In addition, we include a high-volume, bottom-drive aquifer, providing some pressure support and storage volume for displaced reservoir fluids (zone 5, **Table 2**). We generate the additional volume in the bottom 10 m of the reservoir by artificially increasing the capacity of each cell by a factor of 10,000, enabling the layer to accommodate a significant volume of fluid, which can potentially be exchanged with the adjacent layer, zone 4 (**Table 1**).

A well is drilled through the centre of the reservoir and includes a dual completion for different stratigraphic injection and production zones, i.e. the same well can inject and produce H_2 from either the same or different zones of the reservoir. Each completion covers 12 meters of vertical stratigraphy so that we can place both the injection and production completions entirely within zone 2, which is important to observe the impact of the vertical heterogeneity on reservoir performance, including the additional heterogeneity incorporated in the complex models (see below). Completions are placed in one of three positions; at the top (between 1000 m – 1012 m), middle (1035 m – 1047 m) and base (1073 m – 1085 m) of the reservoir. We avoid injecting into the aquifer layer (zone 5). Keeping the production well above or at the same level as the injection well, there are six completion designs for both the basic homogeneous and basic heterogeneous models (see **Figure 3**). These 12 models are called the "baseline models", against which we assess the impact of increased heterogeneity on reservoir performance.

For the next step, we create complex homogeneous and heterogeneous models. To do this heterogeneity is increased in the 12 baseline models by introducing a 1 m thick, low

permeability zone (LPZ) at the base of zone 1 (1034 m – 1035 m) or zone 2 (1047 m – 1048 m) (**Figure 2**). Only one LPZ is activated at a time in different simulations. The layers used for the LPZs are already incorporated into the basic reservoir models used to create the baseline models, so the overall reservoir thickness remains at 95 m. Only the permeability is altered so that the porosity in the LPZ layer and the overall pore volume of the reservoir remains the same as in the baseline models (**Figure 2**).

The permeability of each LPZ is altered in 7 increments of one order of magnitude, from 10^{-5} mD to 10^{1} mD while porosity is fixed at 11.61% for the complex homogeneous models and either 13.55% (LPZ1) or 13.95% (LPZ2) for the complex heterogeneous models. We ran a total of 180 simulations, constituting 15 scenarios for each of the 12 baseline models. The scenarios comprise of all seven permeability increments, for each LPZ position (the complex models) with an additional scenario without any LPZ (the basic model) (**Figure 4**).

Dynamic fluid model

In the absence of relative permeability data for the Navajo sandstone samples, we used a surrogate Brooks-Corey relative permeability relationship in this study (**Figure 5**). The same relationship was used for both drainage and imbibition processes.

We inject the same hydrogen volume (at standard conditions) during each simulation over a four-year, four-month lifetime (7.35 x 10^{8} Sm^3 per injection period, 2.94 x 10^{8} Sm^3 in total). This comprises three injection/production cycles of eight months injection/four months production plus a final eight-month injection/eight-month production cycle. The gas is injected at 300,000 $Sm^3.d^{-1}$ and the production target is 500,000 $Sm^3.d^{-1}$. To inject the required quantity of H_2, the maximum injection BHP limit is 1000 MPa. The minimum BHP for production was set at atmospheric pressure to enable the movement of gas to be observed in simulations with lower permeability. Otherwise well shut-in would occur quickly in these circumstances and would be the main control on the scenarios. On violating the minimum BHP limit, production rates are reduced to ensure that the cycle maximises the overall productivity but remains within the set operational limits.

Results

Baseline scenarios

The cumulative (a) hydrogen and (b) water production over the four cycles for the six well-completion options (**Figure 3**) for each of the basic homogeneous and heterogenous models are shown in **Figure 6**. There are clear differences in the magnitude of H_2 production response with decreasing well depth. The basic homogeneous model demonstrates that the shallower the production well, the higher the cumulative recovery, with the top of the reservoir being the optimal position for the production well. This is expected and takes into account the way hydrogen moves between cycles due to buoyancy effects. However, due to the increased permeability in the upper zone of the basic heterogeneous model the maximum cumulative hydrogen production of 2.79 x 10^8 Sm^3 for all the basic models results from the heterogeneous model with either both injector and producer at the top of the reservoir (HET_T_T – see **Figure 4** for a list of all nomenclature) or the injector in the middle position and producer at the top (HET_M_T) (2.78 x 10^8 Sm^3), about 55% larger than the volumes produced by the homogeneous models (1.80 x 10^8 and 1.79 x 10^8 Sm^3 respectively).

The cumulative water production does not follow the same pattern as gas production for the basic models. Scenario HET_B_T produces the most water (3.04 x 10^5 Sm^3) followed by HOM_B_B. The same configuration in the basic heterogeneous model (HET_B_B) produces the least water overall (4.47 x 10^3 Sm^3) (**Figure 6**b). In the former two scenarios, with high water production (HET_B_T and HOM_B_B), the producer is positioned in a zone with high (HET, 112.36 mD) or reasonably high (HOM, 34.96 mD) permeability and low hydrogen availability, whereas the low water production (HET_B_B) is due to the low permeability (0.315 mD) in zone 4, where the producer is placed.

Bottom hole pressures and produced gas rate are shown in **Figure 7** (basic homogeneous) and **Figure 8** (basic heterogeneous) for the six possible well configurations. The maximum production rate (500,000 $Sm^3.d^{-1}$) is sustained for longest in the basic heterogenous model with both the injector and producer positioned at the top of the reservoir (HET_T_T, **Figure 8)**. The maximum production rate is not achieved in any of the four cycles in either the basic homogeneous or heterogenous models with both the injector and producer at the base of

the reservoir and in the basic heterogeneous model with the injector at the base and the producer in the middle position (**Figures 7** and **8**).

The maximum injection BHP (1000 MPa) is reached in the basic heterogenous models, all where the injector is placed in the layer that has the lowest permeability (zone 4, 0.315 mD) of the three completion positions (**Figure 8**). Almost all scenarios violate the minimum production BHP (atmospheric pressure) in all production cycles. There are two exceptions, both for the basic heterogeneous model with the producer at the top and the injector either at the top or in the middle position of the reservoir (HET_T_T and HET_M_T). These scenarios only avoid the minimum BHP in the third cycle. It is perhaps predictable that the scenarios closest to meeting the required outputs involve the basic heterogeneous model when the layer with the highest permeability is utilised. However, the failures to achieve the target production rate in most of the scenarios highlight the need for additional H_2 or lower production targets for reservoirs with similar pore volumes to be run effectively.

Simulations with increased heterogeneity

The cumulative gas outputs of 108 scenarios are displayed in **Figure 9**. These include 12 baseline scenarios with no LPZs (utilising the basic models) and 96 simulations with increased heterogeneity (either LPZ1 or LPZ2 activated – employing the complex models). The outputs of 72 simulations where the LPZs were either 0.1, 1 or 10 mD are excluded due to their similarity to the baseline scenarios, in particular the integral contrasts within the baseline heterogeneous models and do not provide additional insight into the effect of permeability contrasts on H_2-water flow. The maximum cumulative hydrogen production is 2.82×10^8 Sm^3. This is observed in the complex heterogenous model with the injector and producer at the top of the reservoir and a LPZ1 of 10^{-5} mD (HET_T_T_LPZ1(10^{-5}), **Figure 9**b). The cumulative hydrogen production shows a minimal increase (1.4%) from the maximum production of the baseline HET_T_T, with no LPZs (**Figure 9**b). The highest cumulative hydrogen production in the homogeneous model is 2.78×10^8 Sm^3, also the T_T scenario with a LPZ1 of 10^{-5} mD (HOM_T_T_LPZ1(10^{-5}), **Figure 9**); more than 50% increase from the T_T baseline scenario (1.80×10^8 Sm^3) (**Figure 9**a).

In all scenarios with the injector and producer either side of the LPZ cumulative gas production is reduced when the LPZ ≤ 10^{-2} mD (**Figure 10**). Once the permeability of the LPZ is reduced to 10^{-5} mD there is no gas production (except in the HOM_B_M_LPZ1 scenario). There is also no gas production where the LPZ is 10^{-4} mD in the HOM_M_T_LPZ1, HOM_B_T_LPZ1 and HOM_B_T_LPZ2 scenarios (**Figure 10**).

Discussion

Well position

Although well position was predominantly employed to determine the effects of the heterogeneity in the reservoirs, there are some relevant findings from their inclusion in the study. In the baseline scenarios, well position affects cumulative gas production (**Figure 6**) and the position of the production well is more critical than the injection well. As a result, and due to H_2 buoyancy, the shallower production wells yield more gas. The relationship between the producer position and gas production is best demonstrated when calculating mean production values for all 180 scenarios. These decrease from 1.73 x 10^8 to 0.93 x 10^8 and 0.22 x 10^8 Sm^3 for the top, middle and base position, respectively (**Figure 11**).

In addition, shallower injection wells produce more gas for the same production well position; particularly compare the outcomes of HOM_T_T, HOM_M_T and HOM_B_T (producing 1.80 x 10^8 Sm^3, 1.79 x 10^8 Sm^3 and 1.56 x 10^8 Sm^3 of H_2, respectively), where permeability is not an additional variable (**Figure 6**a). However, the difference between the outputs can be small when (i) both wells are in high permeability zones, (ii) the production well is near the top of the reservoir, and (iii) there are no low permeability barriers in between the wells. Similar outputs for M_T and T_T scenarios for both basic homogeneous and heterogenous models are obtained when all three conditions are fulfilled (**Figure 6**a) in contrast to the outputs for the M_T models with and without LPZ1 activated (**Figure 9**).

Scenarios that do not have the producer at the top of the reservoir produce less gas because buoyancy pushes H_2 above the well position. However, in the scenarios with the producer at the base of the reservoir, the basic heterogeneous model produced more hydrogen than the basic homogeneous model as the low permeability of zone 4 inhibits upward H_2 migration, resulting in 9.8 x 10^5 Sm^3 (HET_B_B) compared to 6.2 x 10^5 Sm^3 (HOM_B_B) (**Figure 7**a). However, the low permeability of zone 4 in the heterogenous model (0.315 mD) significantly hampers hydrogen injection, requiring an unrealistic maximum injection well BHP of 10^3 MPa to inject the required volume of hydrogen. In addition, when hydrogen is injected into the base of the reservoir, a significant proportion flows into the aquifer beneath and is prevented

from returning to the reservoir by the low permeability of zone 4 at the base of the heterogenous model.

Contrasting permeabilities

In our models, hydrogen migration is disrupted by permeabilities of 10^{-2} mD (**Figure 10**). This suggests that even minor heterogeneities in a sandstone reservoir (one order of magnitude in HET_B_T), particularly if they are laterally continuous and extensive, will affect flow, plume development and the withdrawal of hydrogen when cycled. Such heterogeneities could be created by subtle changes in depositional layering, such as fine or silty interdunes in a succession dominated by aeolian dune bedding, or structural features, including zones of deformation bands, which may extend up to hundreds of metres, with permeabilities several orders of magnitude lower than the main reservoir rock (Krystinik, 1990; Mountney, 2011; Pourmalek et al., 2021). Permeabilities of ≤10^{-4} mD create sealing or near sealing layers under the conditions investigated (**Figure 10**), although in some circumstances there is still some flow across LPZs of 10^{-5} mD, indicating that pressure gradient is having an effect in these scenarios.

We find that a permeability contrast of three to four orders of magnitude is needed for reduction in flow, due to the relationship between permeability and viscosity (Equation 1). This is similar to what has been proposed by Ringrose and Bentley (2021). There is a stepped reduction in flow in the M_T_LPZ1 model when the barrier permeability decreases from 10^{-2} to 10^{-3} mD. This transformation point corresponds to a contrast of three and four orders of magnitude lower than the preceding permeability in the reservoir (34.96 and 18.88 mD in the homogenous and heterogeneous models, respectively) (**Figure 10**). When LPZ1 is 10^{-2} mD, over 90% of the heterogeneous baseline (2.53 x 10^8 Sm^3, compared with 2.78 x 10^8 Sm^3 (HET_M_T)) and over 70% of the homogeneous baseline model total (1.28 x 10^8 Sm^3 compared with 1.79 x 10^8 Sm^3 (HOM_M_T)) of hydrogen is produced. An activated LPZ1 of 10^{-3} mD reduces flow to 30% of the heterogenous and 4% of the homogeneous baseline hydrogen production totals, respectively. Therefore, this decrease in permeability can significantly affect reservoir performance.

The relationship between permeability and viscosity (Equation 1) also implies that permeability contrasts do not affect all fluids equally. Although the simulations with the LPZ beneath the injector in either the M_T or T_T scenario generally produce more hydrogen as the LPZ permeability decreases, the results for the simulations with a LPZ of 10^{-3} mD do not fit this pattern (**Figure 12**). This seeming anomaly is created by the flow of fluid across the lower LPZ. In the simulation where the LPZ is 10^{-2} mD, both water and hydrogen can flow across the LPZ so that pressure is dissipated as hydrogen is injected and maintained as hydrogen is produced, creating smaller fluctuations in overall pressure (**Figure 13**). When LPZ permeability is reduced to 10^{-3} mD, water is not able to flow through the barrier easily, so pressure fluctuations are larger as hydrogen is injected and produced (**Figure 13**). As the pressure reduces more quickly than in the 10^{-2} mD simulation, the producer violates the BHP constraint (atmospheric pressure) earlier in the production cycles in the 10^{-3} mD simulation, hence less hydrogen is produced. The comparison of the 10^{-2} mD and 10^{-3} mD scenarios highlight the importance of understanding the flow of all fluids in the reservoir and the timing of injection and production is crucial in balancing reservoir pressure and therefore how it performs in the successive cycles. If the 10^{-3} mD scenario arose it may require a costly recompletion of the well to prevent a similar capacity, injection and potential storage security problems as experienced at the Snøhvit CCS and In Salah CCS demonstration projects (Ringrose et al., 2013; Jenkins et al., 2015).

Compartmentalisation

The combination of low permeability layers and features can create compartments, ranging from reservoir-defining, kilometre-scale structures (e.g. created by faults) to metre-scale features, including deformation bands, with sedimentary processes spanning this scale range (Griffiths et al., 2016; Medici et al., 2019). Our results suggest that compartmentalisation also needs to be considered in relation to the effectiveness of UHS within porous media. The scenarios with the LPZ below both injector and producer (i.e. wells within the same structural compartment), show that activating a LPZ of ≤10^{-2} mD increases the cumulative gas produced in almost all scenarios for both the homogeneous and heterogenous models (**Figure 12**). However, the increase in H_2 production is more dramatic in the homogeneous models. This is because the basic heterogenous model already acts as a compartmentalised reservoir, with

the low permeability of zones 3 and 4 (0.235 and 0.315 mD, respectively) restricting fluid movement (**Figure 14**). This demonstrates the need for a holistic understanding of reservoir structure as fluid flow and plume development are affected by permeability and thickness of all surrounding facies in the reservoir and not just those on the immediate flow paths.

In scenarios that did not have any flow barriers below the injector, we observe that in addition to upward migration, hydrogen flows downwards during injection, even though the well is perforated laterally and gas is injected radially (**Figure 14**). This indicates that when the injector is placed at the base of the reservoir some H_2 flows into deeper aquifer layers (zone 5). We also find downward flow in the basic heterogeneous model by constructing a model with higher permeability in zones 3 and 4. This is because some of the injected H_2 is forced downwards as the cells surrounding the upper portion of the well completion become saturated making lateral and downward movement the most energy efficient pathway. The downward migration is accentuated in our simulations because of the discrepancy in the horizontal and vertical cell size, 100 m and 1 m, respectively. Downward movement of hydrogen was also identified by Lysyy et al. (2021) by simulating injection of hydrogen into gas and oil zones. A consequence of the initial downward movement of hydrogen is increased lateral plume development. The additional lateral movement is generated when hydrogen alters its direction of movement, from downward to upward flow, when buoyancy pressure overcomes downward forces from injection. At the turning point hydrogen encounters the downward-flowing hydrogen, forcing it to move laterally into the adjacent cells as this is the path of least resistance.

The simulations where injector and producer are in the same structural compartment produce the most hydrogen: the highest cumulative quantities of hydrogen are produced by T_T_LPZ1 (10^{-5}), amounting to 2.78 x 10^8 Sm^3 for the homogeneous and 2.82 x 10^8 Sm^3 for the heterogenous model. However, the compartmentalised scenarios also experience some of the highest zonal pressure fluctuations, which increase as the LPZ permeability decreases (**Figure 13**). Pressure fluctuations can facilitate high hydrogen production but also increase stress and strain on the reservoir. This potentially affects subsequent injection and production cycles and might impact on caprock integrity (Fu et al. 2017; Zhou et al. 2023). As such, pressure needs to be carefully monitored within UHS, particularly as many features that form

compartments are below the limits of seismic detection. Use of depleted hydrocarbon fields may mitigate against this potential issue as the structure of a field and flow pathways are better understood, particularly if they have been subject to secondary or tertiary recovery.

Where injector and producer are not in the same compartment, low permeability layers will form a barrier to fluid flow. This will lead to dissipation of the hydrogen plume and gas trapping where there is insufficient column height to create the excess pressure required to migrate across the barrier (see below). The hydrogen trapping may be exacerbated by the low permeability layers preventing the flow of other fluids, potentially creating additional baffles. The effect on other fluids is not only an important consideration in the use of aquifers for UHS but when other fluids, such as methane, carbon dioxide or nitrogen are considered for use as cushion gas (Kanaani et al., 2022; Zamehrian and Sedaee, 2022). Therefore, if the wells are separated by LPZs, the compartments influence the availability of hydrogen and pressure in the reservoir by regulating the flow of fluids through its barriers. As such, in reservoirs affected by compartmentalisation it may be prudent to use the same well for injection and production (Lubon and Tarkowski, 2020).

Pressure and hysteretic effects

Effects on pressure have been discussed in relation to the migration of different fluids across a barrier. However, the pressure gradient is also the impetus for fluid flow, indicated by the migration of hydrogen across a LPZ of 10^{-5} mD (above). The factors controlling the differential either directly relate to the gas pressure gradient below the LPZ, affecting the quantity and focus of H_2 present, or indirectly affect the gas pressure gradient by regulating the presence and production of other fluids, affecting overall reservoir (or compartment) pressure.

The antecedent gas column height controls the pressure gradient below the LPZ. Comparison of the B_T scenarios shows that in both the complex homogeneous and heterogenous models more hydrogen is produced when LPZ1, rather than LPZ2, is activated (**Figure 10**). We demonstrate the reason the LPZ1 simulation has a higher cumulative hydrogen production using the homogeneous model (so the LPZ creates the only permeability contrasts) with LPZs of 10^{-2} mD (as water flow is less affected), where the LPZ1 simulation has a higher total gas

production of 2.37 x 10^7 m^3. When LPZ2 is activated, less hydrogen is available to the producer in zone 1 (**Figure 15**) because when the plume encounters the LPZ earlier, it has an increased lateral spread (**Figure 16**). As a result, hydrogen concentration is lower in the centre of the reservoir and there is more hydrogen at the periphery of the plume (**Figure 16**b, d). As such, more hydrogen becomes trapped below LPZ2 as the hydrogen column height at the margins of the reservoir is too low to create a sufficient pressure gradient for hydrogen to migrate across the LPZ. Conversely, if the LPZ is shallower, and therefore further away from the injector (**Figure 16**a, c), hydrogen predominantly remains in the centre of the reservoir until it reaches the LPZ. In this scenario, a greater gas column height results in a higher pressure gradient beneath the LPZ. The scenario with LPZ1 activated is then in a better position to take advantage of the biggest pressure drop across the LPZ during the production cycle. **Figure 15** shows that during the production cycles in the LPZ1 scenario, the hydrogen in zone 1 is replaced quicker than it is produced in cycle 1 and nearly as quickly as it is produced in the other cycles, whereas in the LPZ2 scenario there is a greater drop in hydrogen volume in zone 1 during production cycles. It may be that the column height phenomenon is lessened by numerous cycles, when the eventual accumulation of gas in the LPZ2 case creates enough pressure to migrate across the barrier, or by longer shut-in periods in-between the injection and production cycles, as the gas will rise and equilibrate below the LPZ prior to production.

In addition to the increased pressures caused by the gas column height, there is an increased hysteretic effect in the LPZ1 scenario. This is because the cells across the LPZ experience higher hydrogen saturation, enabling the hydrogen flow rate across the LPZ in successive migration to be maintained at lower pressures (**Figure 5**). This form of hysteresis may be crucial to UHS as Wang et al. (2022) found that the piston-like movement of cushion gas during H_2 production, referred to as sweep efficiency, was not the main mechanism by which H_2 was recovered. Instead, the hydrogen migrated back along the flow paths utilised during injection, increasing the importance of processes, such as hysteresis, that affect the gas permeability along these pathways.

Implications for UHS optimisation

In addition to the relationship between permeability and viscosity, local pressure factors governed by gas column heights, environmental pressures controlled by compartmentalisation and the flow and production of other fluids in the reservoir, as well as hysteretic effects explain the behaviour of gas in relation to the permeability contrasts encountered in our reservoir simulations. The results show that it is not sufficient to consider permeability contrasts in isolation and the reservoir system must be viewed holistically to understand how flow patterns control plume development.

Overall, when the LPZs are introduced, there are some broad similarities in responses of the complex homogeneous and heterogeneous models; all simulations produce less gas than the baseline scenarios when the LPZ is in between the wells and almost all simulations produce more gas than the baseline scenarios when the reservoir is compartmentalised and the wells are in the same compartment. However, due to the combination of permeability contrasts, the LPZs also amplify some of the differences in the homogeneous and heterogeneous reservoir structures. For instance, the cumulative gas outputs reflect the usage of the respective higher permeability layers of the reservoirs, such that, the reservoirs based upon the homogeneous model produce more hydrogen when the base of the reservoir is utilised for one or both of the wells, whereas the complex heterogeneous simulations recover more gas when the top of the reservoir is utilised for one or both of the wells.

The M_M scenarios also reflect the permeability differences. Of the two LPZ positions, the complex homogeneous models produce more hydrogen in the LPZ2 scenarios and the complex heterogeneous models produce more gas in all LPZ1 simulations. In both scenarios, the higher permeability above the wells, or surrounding the well when the well is at the effective reservoir top in the M_M_LPZ1 scenario, allows increased lateral plume spreading so that less gas is available for production. The lower H_2 production for the homogeneous reservoir in the LPZ1 scenario is compounded by more gas being able to flow downwards into the base layers. This explains why the HOM_M_M_LPZ1 gas outputs are similar for the four LPZ permeabilities, as similar quantities of gas flow downwards, then migrate back upward (mechanism described above) and can be produced over the four cycles. However, the heterogeneous reservoir (HET_M_M_LPZ1) acts more similarly to the homogeneous T_T

scenarios with either of the LPZs activated and produces increasingly more gas as the compartment becomes tighter (**Figure 9**).

In relation to the compartmentalised scenarios, the cumulative gas outputs are very similar for the lowest permeability (LPZ of 10^{-5} mD) T_T_LPZ1/2 and M_T_LPZ2 scenarios, despite the homogeneous model having just over a quarter of the permeability in zone 1, i.e. 35 mD compared with 112 mD (**Figure 12**). This suggests that for pre-set production rates there are diminishing yields for hydrogen production once permeability has increased above a certain level (tens of mD in this study for a production rate of 500,000 $Sm^3.d^{-1}$), provided that pore volume is sufficient to accommodate the required hydrogen. Therefore, it may be possible to operate UHS in lower permeability storage sites if the required hydrogen production rate is reduced. However, compartmentalisation also impacts upon effective reservoir size, potentially causing problems similar to those experienced at the CO_2 storage test site at Snøhvit and ultimately reducing storage capacity (Jenkins et al., 2015). Some of these issues can be mitigated by injection-production regime, as discussed below.

As we have shown, heterogeneity affects the pressure experienced in a reservoir by affecting fluid movement. This creates a circular relationship because pressure gradient dictates how the fluids interact with permeability contrasts. Operational tools, such as the length of the injection and production cycles, including any shut-in periods, and the injection and production rates, along with the use of cushion gas (not discussed in this study), can be used to overcome some of the pressure issues and control flow within the reservoir (Lubon and Tarkowski, 2020; Mahdi et al., 2021). These mechanisms can also be used to manage the storage facility, either recovering the maximum amount of hydrogen (recovery factor), ensuring a timely meeting of energy demand, or managing the purity of the recovered H_2 (Lubon and Tarkowski, 2020; Kanaani et al., 2022; Wang et al., 2022; Bo et al., 2023). It will be necessary to decide which of these three, potentially competing, outputs from a reservoir is the overarching objective to implement the most effective management strategy. It may be that a range of reservoir management strategies can be produced, based-upon the nature or timeliness of end use, which can then be tailored to each reservoir.

Although our models are not sufficiently complex to induce viscous fingering, we can infer that coupling of some of the observed processes may create this effect in a more heterogeneous reservoir. For instance, the lateral plume development from the downward injection initially reduces the plume's intensity. If this plume, with lower gas concentration, then encounters low permeability features, it is less likely to be able to migrate across them, creating further lateral movement. This is particularly the case if there is better lateral than vertical connectivity. In an anisotropic reservoir with multidirectional plume development and numerous permeability contrasts, the hydrogen plume is likely to lose its integrity, creating different pathways as it migrates upwards. Multiple pathways increase the likelihood of trapping, as the pressure gradient is reduced if the plume is separated. However, much of the plume coherence may be recaptured if hydrogen accumulates at the top of an anticlinal structure (Zamehrian and Sedaee, 2022; Bo et al. 2023). In general, it is most effective for both the injector and producer to be placed at the top of the reservoir. However, having a separate injector may prove beneficial to regulate pressure around the wells, so that it is not necessary to inject hydrogen into a smaller volume at the top of an anticline, although there is obviously a cost implication to having separate wells.

In addition to selecting the most appropriate well location for the reservoir structure, our findings from the simple models with escalating heterogeneities underline the need to understand the sedimentary and structural geology that create the permeability contrasts throughout the entirety of the reservoir. This study demonstrates that features that are lateral and continuous will affect the fluid flow and therefore the efficacy of a potential storage system. As discussed, the features affecting permeability within the reservoir can either be sedimentary or structural. Some of the reservoir architecture will be detected by seismic surveys, however, many impactful features are below seismic detection limits, such as thin beds within a layer-cake architecture or zones of deformation bands (Ringrose and Bentley 2021; Wakefield et al., 2022). Further work is needed to determine how fluid flow is impacted by this range of features to determine whether they significantly affect the efficacy of UHS in clastic reservoirs. Answers arising from this research will inform the type and frequency of sampling needed to obtain the resolution required, or in other terms, the complexity needed for effective modelling and the day-to-day operational management of the reservoir.

Finally, in this study we show that hysteretic effects prove beneficial to hydrogen flow, allowing the gas to flow more easily along previously established pathways. In addition, it may be that hysteretic effects over multiple cycles prevent plume dispersal, improving the recovery factor (Zhang et al., 2023). However, several studies using different relative permeability relationships for drainage and imbibition and incorporating trapping into subsequent cycles, have predicted that hysteresis reduces working gas capacity, H_2 recovery factor and has a negative effect on injection and production rates (Wang et al., 2022; Bo et al., 2023; Lysyy et al., 2023; Pan et al., 2023). This is because the phases trapped in the reservoir at the end of the injection and production cycles are immobile. However, this may not substantially impact upon the hydrogen recovery (Wang et al., 2022). More experimental work is needed in relation to this process and its effects.

Conclusions

By introducing increasing heterogeneities into simple reservoir models, we found that, due to the buoyancy of H_2, wells placed higher up in the reservoir produce more gas. In addition, permeabilities of $\leq 10^{-2}$ mD disrupt the flow of H_2 and lower permeability of $\leq 10^{-4}$ mD create near-no flow barriers.

Similar to predictions, permeability contrasts of three to four orders of magnitude significantly affect flow, however, factors affecting the pressure gradient also needed to be considered. These factors include compartmentalisation, the effect of permeability on the flow of co-existing fluids (which in themselves can create additional baffles) and the localised pressure gradient created by the H_2 plume. We have demonstrated some of the fundamental processes of fluid pathway development using simple models, providing insights that can be applied to more complex UHS investigations.

We have shown that reservoirs with lower permeability (35 mD) can work almost as effectively as storage with higher permeability (112 mD) if injection and production demands are not too high and there is sufficient pore space for fluid storage. Lower permeability also reduces lateral spreading and may improve the hydrogen recovery factor. Likewise, some of the issues created by permeability contrasts, such as dispersal of the hydrogen plume and

structural trapping, can be mitigated by operational reservoir management, such as well placement, controlling injection and production rates or shut-in times. Although not studied in this research, the use of cushion gas is another tool that can assist in managing the reservoir effectively. However, our research underlines the need to understand the architecture of the whole reservoir, not just the zones surrounding the wells and pathways in-between, as this controls capacity, pressure fluctuations and informs operational management decisions. It also highlights the need for further research about how heterogeneities across different scales, particularly those that are below sub-seismic detection, affect fluid flow and therefore the efficacy of UHS in sedimentary reservoirs.

Acknowledgements

This work was supported by the Natural Environment Research Council via an IAPETUS2 PhD studentship held by D Smith (grant reference NE/S007431/1).

Edward Hough publishes with permission of the Executive Director of the British Geological Survey (BGS-UKRI).

References

Aftab, A., Hassanpouryouzband, A., Xie, Q., Machuca,L.L. and Sarmadivaleh, M. (2022) Toward a Fundamental Understanding of Geological Hydrogen Storage, Ind. Eng. Chem. Res. 2022, 61, 3233−3253, https://doi.org/10.1021/acs.iecr.1c04380.

Amirthan, T., Perera, M.S.A. (2022) The role of storage systems in hydrogen economy: A review, Journal of Natural Gas Science and Engineering 108 (2022) 104843, https://doi.org/10.1016/j.jngse.2022.104843.

Arekhov, V., Clemens, T., Wegner, J., Abdelmoula, M., Manai, T. (2023) The Role of Diffusion on Reservoir Performance in Underground Hydrogen Storage, SPE reservoir evaluation & engineering, 26(4), pp. 1566–1582, https://doi.org/10.2118/214435-PA.

AusGov (2019) Australia's National Hydrogen Strategy [online]. https://www.dcceew.gov.au/sites/default/files/documents/australias-national-hydrogen-strategy.pdf (accessed on 21 October 2022).

Barua, A. K., Afzal, M., Flynn, G. P. and Ross, J. (1964) Viscosity of Hydrogen, Deuterium, Methane, and Carbon Monoxide from — 50° to 150°C below 200 Atmospheres, J. Chem. Phys. 41, 374 (1964); https://doi.org/10.1063/1.1725877.

Bo, Z., Boon, M., Hajibeygi, H., Hurter, S. (2023) Impact of experimentally measured relative permeability hysteresis on reservoir-scale performance of underground hydrogen storage (UHS), International Journal of Hydrogen Energy, 48, Issue 36, 29 April 2023, Pp 13527-13542, https://doi.org/10.1016/j.ijhydene.2022.12.270.

Boon, M., Hajibeygi, H.(2022) Experimental characterization of H_2/water multiphase flow in heterogeneous sandstone rock at the core scale relevant for underground hydrogen storage (UHS), Scientifc Reports (2022) 12:14604, https://doi.org/10.1038/s41598-022-18759-8.

Cedigaz (2020) Underground gas storage in the world – 2020 status [online]. Available at https://www.cedigaz.org/underground-gas-storage-in-the-world-2020-status/ (accessed on 23 December 2021).

Chai, M., Chen, Z., Nourozieh, H., Yang, M. (2023) Numerical simulation of large-scale seasonal hydrogen storage in an anticline aquifer: A case study capturing hydrogen interactions and cushion gas injection, Applied Energy 334 (2023) 120655, https://doi.org/10.1016/j.apenergy.2023.120655.

de Coninck, H., Revi, A., Babiker, M., Bertoldi, P., Buckeridge, M., Cartwright, A., Dong, W., Ford, J., Fuss, S., Hourcade, J. C., Ley, D., Mechler, R., Newman, P., Revokatova, A., Schultz, S., Steg, L., & Sugiyama, T. (2018). Strengthening and Implementing the Global Response. In Global warming of 1.5°C: Summary for policy makers (pp. 313-443). IPCC - The Intergovernmental Panel on Climate Change

Feldmann, F., Hagemann, B. Ganzer, L., Panfilov, M. (2016) Numerical simulation of hydrodynamic and gas mixing processes in underground hydrogen storages, Environ Earth Sci, 75:1165, DOI 10.1007/s12665-016-5948-z.

Fu, P., Settgast, R.R., Hao, T., Morris, J.P., Ryerson, F.J. (2017) The Influence of Hydraulic Fracturing on Carbon Storage Performance, Journal of Geophysical Research: Solid Earth, 122, 9931–9949, https://doi.org/10.1002/2017JB014942.

Gasanzade, F., Tilmann Pfeiffer, W., Witte, F., Tuschy, I. and Bauer, S. (2021) Subsurface renewable energy storage capacity for hydrogen, methane and compressed air – A performance assessment study from the North German Basin, Renewable and Sustainable Energy Reviews 149 (2021) 111422, https://doi.org/10.1016/j.rser.2021.111422.

Griffiths, J., Faulkner, D.R., Edwards, A.P., Worden, R.H. (2016) Deformation band development as a function of intrinsic host-rock properties in Triassic Sherwood Sandstone, Geological Society, London, Special Publications, 435, 161-176, https://doi.org/10.1144/SP435.11.

Hashemi, L., Blunt, M. and Hajibeygi, H. (2021) Pore-scale modelling and sensitivity analyses of hydrogen-brine multiphase flow in geological porous media, Sci Rep 11, 8348 (2021), https://doi.org/10.1038/s41598-021-87490-7.

Heinemann, N., Alcalde, J., Miocic, J.M., Hangx, S.J.T., Kallmeyer, J., Ostertag-Henning, C., Hassanpouryouzband, A., Thaysen, E.M., Strobel, G.J., Schmidt-Hattenberger, C., Edlmann, K., Wilkinson, M., Bentham, M., Haszeldine, R.S., Carbonell, R. and Rudloff, A. (2021) Enabling large-scale hydrogen storage in porous media – the scientific challenges, Energy Environ. Sci., 2021, 14, 853, DOI: 10.1039/d0ee03536j.

Hydrogen TCP-Task 42 (2023), Underground Hydrogen Storage: Technology Monitor Report [online]. Available at https://www.ieahydrogen.org/task/task-42-underground-hydrogen-storage/ (accessed on 31 July 2023).

IEA (2021) Hydrogen: Tracking report – November 2021 [online]. Available at https://www.iea.org/reports/hydrogen (accessed on 7 December 2021).

IEA (2023a) Global Hydrogen Review [online]. Available at https://www.iea.org/reports/global-hydrogen-review-2023 (accessed on 14 December 2023).

IEA (2023b) Net Zero Roadmap: A Global Pathway to Keep the 1.5 °C Goal in Reach [online]. Available at https://www.iea.org/reports/net-zero-roadmap-a-global-pathway-to-keep-the-15-0c-goal-in-reach (accessed on 14 December 2023).

Jangda, Z., Menke, H., Busch, A., Geiger, S., Bultreys, T., Singh, K. (2023) Subsurface hydrogen storage controlled by small-scale rock heterogeneities [online]. Available at https://doi.org/10.48550/arXiv.2310.05302 (accessed on 10 October 2023).

Jenkins, C., Chadwick, A., Hovorka, S.D. (2015) The state of the art in monitoring and verification—Ten years on, International Journal of Greenhouse Gas Control 40 (2015) 312–349, http://dx.doi.org/10.1016/j.ijggc.2015.05.009 (accessed on 20 August 2023).

Kampman, N., Bickle, M.J., Maskell, A., Chapman, H.J., Evans, J.P., Purser, G., Zhou, Z., Schaller, M.F., Gattacceca, J.C., Bertier, P., Chen, F., Turchyn, A.V., Assayag, N., Rochelle, C., Ballentine, C.J., Busch, A. (2014) Drilling and sampling a natural CO_2 reservoir: Implications for fluid flow and CO_2-fluid–rock reactions during CO_2 migration through the overburden, Chemical Geology, 369 (0), 51–82, http://dx.doi.org/10.1016/j.chemgeo.2013.11.015.

Kanaani, M., Sedaee, B., Asadian-Pakfar, M. (2022) Role of Cushion Gas on Underground Hydrogen Storage in Depleted Oil Reservoirs, Journal of Energy Storage, 45, 103783, https://doi.org/10.1016/j.est.2021.103783.

Krystinik, L.F. (1990) Development geology in eolian reservoirs. In: Modern and Ancient Aeolian Deposits: Petroleum Exploration and Production (Eds S.G. Fryberger, L.F. Krystinik and C.J. Schenk), pp. 13-1–13-12. SEPM, Denver.

Lawrence, A., Stuart, M., Cheney, C., Jones, N., Moss, R. (2006) Investigating the scale of structural controls on chlorinated hydrocarbon distributions in the fractured-porous unsaturated zone of a sandstone aquifer in the UK, Hydrogeol J 14, 1470–1482 (2006), https://doi.org/10.1007/s10040-006-0068-6.

Leveille, G.P., Knipe, R., More, C., Ellis, D., Dudley, G., Jones, G., Fisher, Q.J., Allinson, G., 1997. Compartmentalization of Rotliegendes gas reservoirs by sealing faults, Jupiter Fields Area, Southern North Sea. Lond. Special Publ. 123 (1), 87–104, https://doi.org/10.1144/GSL.SP.1997.123.01.06.

LKAB (2022) HYBRIT: Milestone reached – pilot facility for hydrogen storage up and running [online]. Available at https://lkab.com/en/press/hybrit-milestone-reached-pilot-facility-for-hydrogen-storage-up-and-running/#:~:text=In%20May%202021%2C%20construction%20began,operation%20in%20late%20summer%202022 (accessed on 31 July 2023).

Lubon, K., Tarkowski, R. (2020) Numerical simulation of hydrogen injection and withdrawal to and from a deep aquifer in NW Poland, International journal of hydrogen energy, 45, 2068-2083, https://doi.org/10.1016/j.ijhydene.2019.11.055.

Lysyy, M., Fernø, M., Ersland, G. (2021) Seasonal hydrogen storage in a depleted oil and gas field, International journal of hydrogen energy, 46, 25160-25174, https://doi.org/10.1016/j.ijhydene.2021.05.030.

Lysyy, M., Fernø, M.A., Ersland, G. (2023) Effect of relative permeability hysteresis on reservoir simulation of underground hydrogen storage in an offshore aquifer, Journal of Energy Storage 64 (2023) 107229, https://doi.org/10.1016/j.est.2023.107229.

Mahdi, D.S., Al-Khdheeawi, E.A., Yujie Yuan, Y., Zhang, Y., Iglauer, S. (2021) Hydrogen underground storage efficiency in a heterogeneous sandstone reservoir, Advances in Geo-Energy Research, 5(4): 437-443, http://dx.doi.org/10.46690/ager.2021.04.08.

Medici, G., Jared West, L., Mountney, N.P., Welch, M. (2019) Permeability of rock discontinuities and faults in the Triassic Sherwood Sandstone Group (UK): insights for management of fluvio-aeolian aquifers worldwide, Hydrogeology Journal (2019) 27:2835–2855, https://doi.org/10.1007/s10040-019-02035-7.

Miocic, J. M., Heinemann, N., Edlmann, K., Scafidi, J., Molaei, F., Alcalde, J. (2023) Underground hydrogen storage: a review, From: Miocic, J. M., Heinemann, N., Edlmann, K., Alcalde, J. and Schultz, R. A. (eds) Enabling Secure Subsurface Storage in Future Energy Systems. Geological Society, London, Special Publications, 528, https://doi.org/10.1144/SP528-2022-88.

Mohamed, E. A., Worden, R. H. (2006) Groundwater compartmentalisation: a water table height and geochemical analysis of the structural controls on the subdivision of a major aquifer, the Sherwood Sandstone, Merseyside, UK, Hydrol. Earth Syst. Sci., 10, 49–64, https://doi.org/10.5194/hess-10-49-2006.

Mouli-Castillo, J., Heinemann, N. and Edlmann, K. (2021) Mapping geological hydrogen storage capacity and regional heating demands: An applied UK case study, Applied Energy 283; 116348, https://doi.org/10.1016/j.apenergy.2020.116348.

Mountney, N. P. (2011). A stratigraphic model to account for complexity in aeolian dune and interdune successions, Sedimentology, 59, 964–989, https://doi.org/10.1111/j.1365-3091.2011.01287.x.

Muhammed, N.S., Haq, B., Al Shehri, D., Al-Ahmed, A., Rahman, M.M., Zaman, E. (2022) A review on underground hydrogen storage: Insight into geological sites, influencing factors and future outlook, Energy Reports 8 (2022) 461–499, https://doi.org/10.1016/j.egyr.2021.12.002.

Pan B., Yin, X., Ju, Y., Iglauer, S. (2021) Underground hydrogen storage: Influencing parameters and future outlook, Advances in Colloid and Interface Science 294 (2021) 102473, https://doi.org/10.1016/j.cis.2021.102473.

Pan, B., Liu, K., Ren, B., Zhang, M., Ju, Y., Gu, J., Zhang, X., Clarksong, C.R., Edlmann, K., Zhu, W., Iglauer, S. (2023) Impacts of relative permeability hysteresis, wettability, and injection/withdrawal schemes on underground hydrogen storage in saline aquifers, Fuel 333 (2023) 126516, https://doi.org/10.1016/j.fuel.2022.126516.

Pei, M., Petäjäniemi, M., Regnell, A. & Wijk, O. (2020) Toward a Fossil Free Future with HYBRIT: Development of Iron and Steelmaking Technology in Sweden and Finland, Metals 2020, 10, 972, https://doi.org/10.3390/met10070972.

Pfeiffer, W.T., Hagrey, SA., al., Köhn, D., Rabbel, W., Bauer, S. (2016) Porous media hydrogen storage at a synthetic, heterogeneous field site: numerical simulation of storage operation and geophysical monitoring. Environ. Earth Sci. 75, http://dx.doi.org/10.1007/s12665-016-5958-x.

Pfeiffer, W.T., Beyer, C., Bauer, S. (2017) Hydrogen storage in a heterogeneous sandstone formation: dimensioning and induced hydraulic effects, Petroleum Geoscience, 23, 315-326, https://doi.org/10.1144/petgeo2016-050.

Pourmalek, A., Newell, A. J., Shariatipour, S. M., Butcher, A. S., Milodowski, A. E., Bagheri, M., Wood, A. M. (2021) Deformation bands in high-porosity sandstones: Do they help or hinder CO_2 migration and storage in geological formations? International Journal of Greenhouse Gas Control 107 (2021) 103292, https://doi.org/10.1016/j.ijggc.2021.103292.

RAG (2023) Underground Sun Storage 2030 [online]. Available at https://www.uss-2030.at/en/ (accessed on 14 December 2023).

Robinson, D.B., Peng, D.Y. (1978) The characterization of the heptanes and heavier fractions for the GPA Peng–Robinson programs, Gas processors association, Research report RR-28.

Ringrose, P. S., Mathieson, A. S., Wright, I. W., Selama, F., Hansen, O., Bissell, R., Saoula, N. & Midgley, J. (2013) The In Salah CO2 storage project: lessons learned and knowledge transfer, Energy Procedia 37 (2013) 6226– 6236, https://doi.org/10.1016/j.egypro.2013.06.551.

Ringrose, P., Bentley, M. (2021) Reservoir Model Design: A Practitioner's Guide (Second Edition), Springer Nature, Switzerland. https://doi.org/10.1007/978-3-030-70163-5.

Scafidi, J., Wilkinson, M., Gilfillan, S.M.V., Heinemann, N., Haszeldine, R.S (2021) Quantitative assessment of the hydrogen storage capacity of the UK continental shelf. International journal of hydrogen energy 46 (2021) 8629-8639, https://doi.org/10.1016/j.ijhydene.2020.12.106.

Tarkowski, R (2019) Underground hydrogen storage: Characteristics and prospects, Renewable and Sustainable Energy Reviews, vol 105, May 2019, pp 86-94, https://doi.org/10.1016/j.rser.2019.01.051.

UKGov (2020a) The Ten Point Plan for a Green Industrial Revolution [online]. Available at https://www.gov.uk/government/publications/the-ten-point-plan-for-a-green-industrial-revolution (accessed on 19 November 2021).

UKGov (2021) UK Hydrogen Strategy [online]. Available at https://www.gov.uk/government/publications/uk-hydrogen-strategy (accessed 19 November 2021).

USGov (2021) The Long-Term Strategy of the United States: Pathways to Net-Zero Greenhouse Gas Emissions by 2050 [online]. Available at https://www.whitehouse.gov/wp-content/uploads/2021/10/US-Long-Term-Strategy.pdf (accessed 7 December 2021).

Wakefield, O.J.W., Hough, E., Hennissen, J.A.I., Thompson, J., Cripps, C., Parkes, D. (2022) Lithofacies control on the formation of deformation bands: an example from the Sherwood Sandstone Group (Induan–Anisian, Lower Triassic) in Western England, AAPG Bulletin (2022) 106 (6): 1301–1324, https://doi.org/10.1306/02032218027.

Wang, G., Pickup, G., Sorbie, K., Mackay, E. (2022) Scaling analysis of hydrogen flow with carbon dioxide cushion gas in subsurface heterogeneous porous media, International Journal of hydrogen energy 47 (2022) 1752-1764, https://doi.org/10.1016/j.ijhydene.2021.10.224.

Zamehrian, M., Sedaee, B. (2022) Underground hydrogen storage in a partially depleted gas condensate reservoir: Influence of cushion gas, Journal of Petroleum Science and Engineering, 212, 110304, https://doi.org/10.1016/j.petrol.2022.110304.

Zhang, H., Zhang, Y., Al Kobaisi, M., Iglauer, S., Arif, M. (2023) Effect of cyclic hysteretic multiphase flow on underground hydrogen storage: A numerical investigation, International Journal of Hydrogen Energy, https://doi.org/10.1016/j.ijhydene.2023.08.169.

Zhou, J., Deng, G., Tian, S., Xian, X., Yang, K., Zhang, C., Dong, Z., (2023) Experimental study on the permeability variation of sandstone at cyclic stress: Implication for underground gas storage, Journal of Energy Storage 60 (2023) 106677 https://doi.org/10.1016/j.est.2023.106677.

Figure 1 Digitised core log of Navajo sandstone from borehole CO_2W55 with the approximate zonation of the analogue for the geological models shown. The approximate location of the porosity and permeability measurements, taken from core samples, are also shown (red writing within the dashed grey rectangle). Adapted from Kampman et al. (2014) © 2014, with permission from Elsevier. Porosity and permeability values that have been determined with a standard device using nitrogen as a working fluid. These values were the basis for the porosity and permeability values used in the geological models.

Figure 2 3D representations of the permeability distribution in the two basic models: a) homogeneous and b) heterogeneous. See **Table 2** for more information about the zones. The dark blue horizontal lines indicate where the low permeability zones (LPZs) are positioned in the second part of the study, although only one LPZ is activated at a time.

Figure 3 Six configurations of the well positions shown in the basic heterogeneous model. The zonal colours relate to the permeability of each layer. The green zone at the base is zone 5, the aquifer-like zone.

Figure 4 Schematic of the 180 simulations run for this study. These include the 12 'baseline scenarios' (highlighted in the shaded blue box) and 168 scenarios where either LPZ1 or LPZ2 is activated (the two ranks of downward pointing arrows at the base of the tree). The downward pointing arrows relate to each of the seven permeability options for the LPZ displayed in the box outlined in red (magnified in the larger rectangle, also outlined in red). Clarification of the nomenclature used throughout the study are also included in this figure.

Figure 5 Relative permeabilities of hydrogen (red line) and water (blue line) used in simulations. The same relative permeability relationship was used for both drainage and imbibition processes.

Figure 6 Outputs from the baseline scenarios a) cumulative gas and b) cumulative water production. There were six variations of well position (B – Base, M – Middle and T – Top), the injector position is recorded first, for each of the homogenous (triangles) and heterogeneous (circles) models.

Figure 6 Gas production rate, injection well BHP and production well BHP for the six basic homogeneous models described by their injector position and then producer position. The hydrogen injection target was 300,000 $Sm^3.d^{-1}$ for 8 months in each of the four annual cycles.

Figure 7 Gas production rate, injection well BHP and production well BHP for the six basic heterogeneous models described by their injector position and then producer position. The hydrogen injection target was 300,000 $Sm^3.d^{-1}$ for 8 months in each of the four annual cycles.

Figure 8 The cumulative gas outputs of 54 simulations each for a) the homogeneous model and b) the heterogeneous model. Note that these charts do not include the outputs for the simulations where the low permeability zones are either 0.1, 1 or 10 mD. For comparison, the black bar marked as "No LPZ" in the legend corresponds to the baseline scenarios.

Figure 9 Outputs of the simulations where the LPZ is in between the injector and producer (B_M_LPZ2, B_T_LPZ1 and LPZ2, M_T_LPZ1) for a) the homogenous and b) the heterogeneous model. For comparison, the black bar marked as "No LPZ" in the legend corresponds to the baseline scenario.

Figure 10 Distribution of the cumulative hydrogen production from all simulations in relation to the position of the producing well. Red points indicate mean values; black horizontal lines are median values; whiskers are 1.5 times the standard deviation; black points are outliers. The blue shapes highlight the outcomes from the baseline models.

Figure 11 Outputs of the simulations where the LPZ is below the injector and producer (M_T_LPZ1 and T_T_LPZ1 and LPZ2) for the a) homogenous model and b) heterogenous model. For comparison, the black bar marked as "No LPZ" in the legend corresponds to the baseline scenario.

Figure 12 Pressure fluctuations in homogeneous model with injector in the middle position and producer at the top with LPZ2 activated (M_T_LPZ2). As the permeability of the LPZ decreases from 10^{-2} to 10^{-5} mD, the pressure fluctuations increase. The grey dashed line shows the periods of hydrogen injection.

Figure 13 Plume development during the first month of the first cycle of hydrogen injection in the (a) basic homogeneous and (b) basic heterogenous model where the injector is placed in the middle of the reservoir. Blue indicates water and the intensity of the pink indicates the saturation of hydrogen in each cell. The white dashed lines indicate the different layers within the heterogeneous model.

Figure 14 Hydrogen available to the producer in the homogeneous model (zone 1) where the injector is at the base and the producer is at the top of the reservoir (B_T). The solid red line shows the simulation with LPZ1 activated and the blue dashed line shows the simulation with LPZ2 activated. In both instances the LPZ has a permeability of 10^{-2} mD. The grey dashed line shows the injection cycles, for reference.

Figure 15 Comparison of lateral hydrogen plume migration during the first injection cycle in the homogeneous simulations, where the injector is at the base and the producer at the top of the reservoir (HOM_B_T). Both simulations have a LPZ of 10^{-2} mD. a) LPZ1 is activated; b) LPZ2 is activated. c) and d) are expanded segments of a) and b), respectively and the orange ellipse highlights the lateral movement of hydrogen in the equivalent cell below the LPZ. Blue indicates water and the intensity of

the pink indicates the saturation of hydrogen in each cell. The white dashed line illustrates the position of the activated LPZ.

Table 1 Shared properties of the basic models. The injection and production flow rates are based upon volumes at standard (atmospheric) pressure.

Parameter	Value
Dimensions	1500 m x 1500 m x 95 m
Cell number (i x j x k)	15 x 15 x 95
Cell volume multiplier for lowest 10 rows	10,000
Depth range	1000 m – 1095 m
Initial pressure at 1000 m depth	10 MPa
Reservoir temperature	50 °C
Rock compressibility	5.8×10^{-4} MPa^{-1}
Average porosity	11.64%
Average permeability (excl. low permeability layers)	34.96 mD
Initial water saturation	100%
Injection rate	300 000 Sm^3 d^{-1}
Target withdrawal rate	500 000 Sm^3 d^{-1}
Dip of strata	0° (horizontal)

Table 2 Properties of zones 1-4 that act as the reservoir for the basic heterogeneous model. Zone 5 is an aquifer-like zone at the base of the reservoir, in which the volume of the cells in zone 5 were enlarged by a factor of 10,000. The overall thickness, including the aquifer, was 95 m.

Zone	Thickness (m)	Porosity (%)	Permeability (mD)
1	35	13.55	112.36
2	13	13.95	18.88
3	7	9.07	0.235
4	30	11.61	0.315
5	10	11.64	34.96

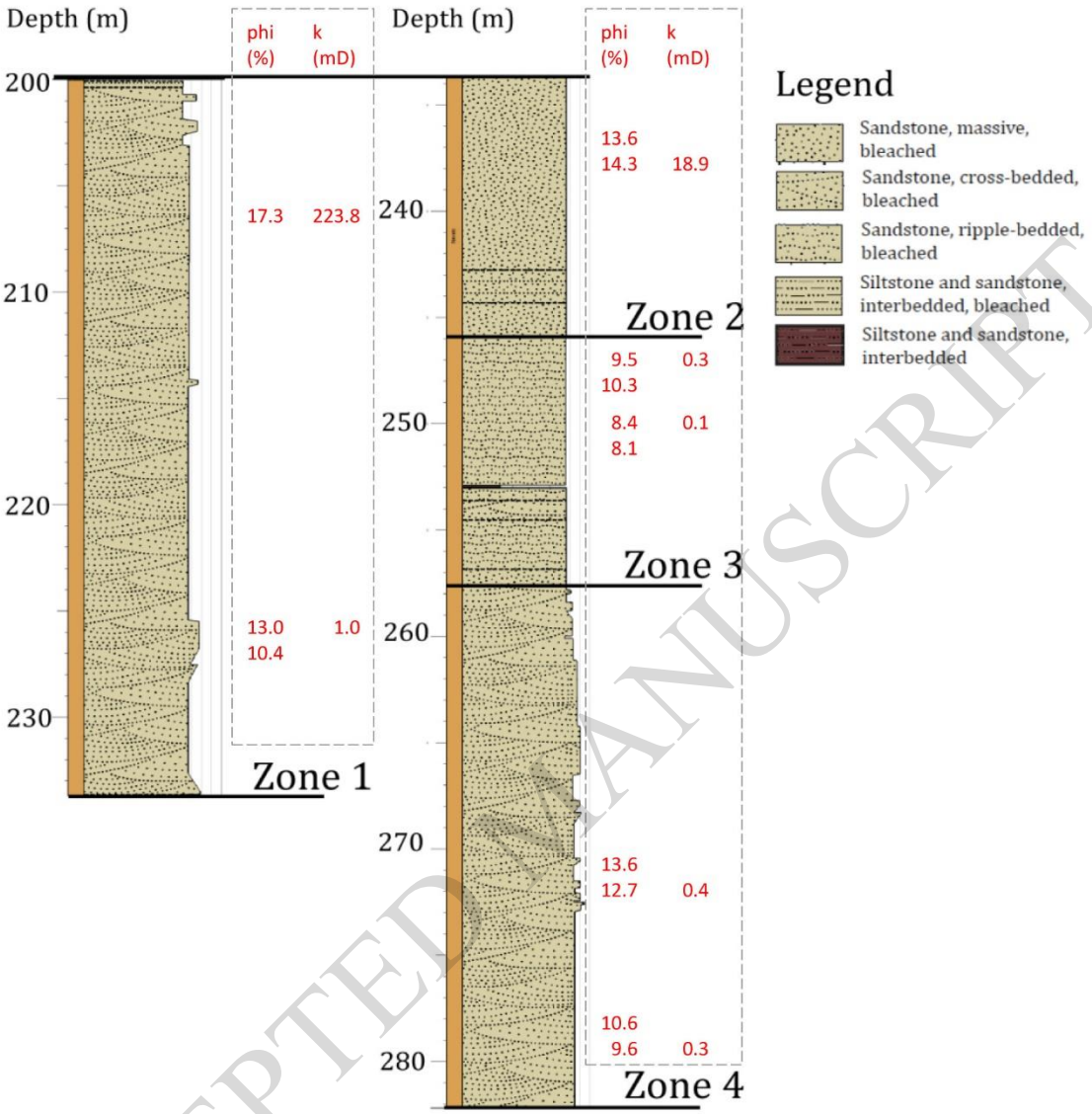

Figure 1

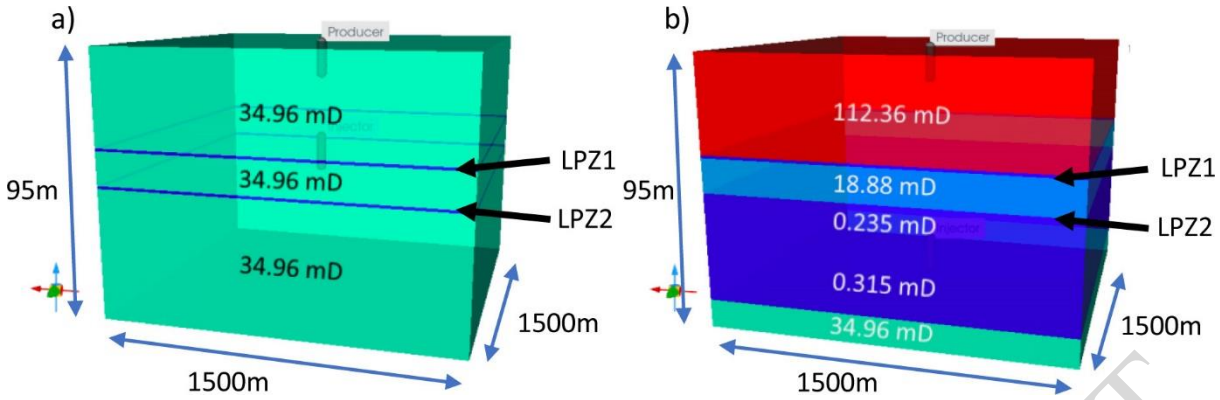

Figure 2

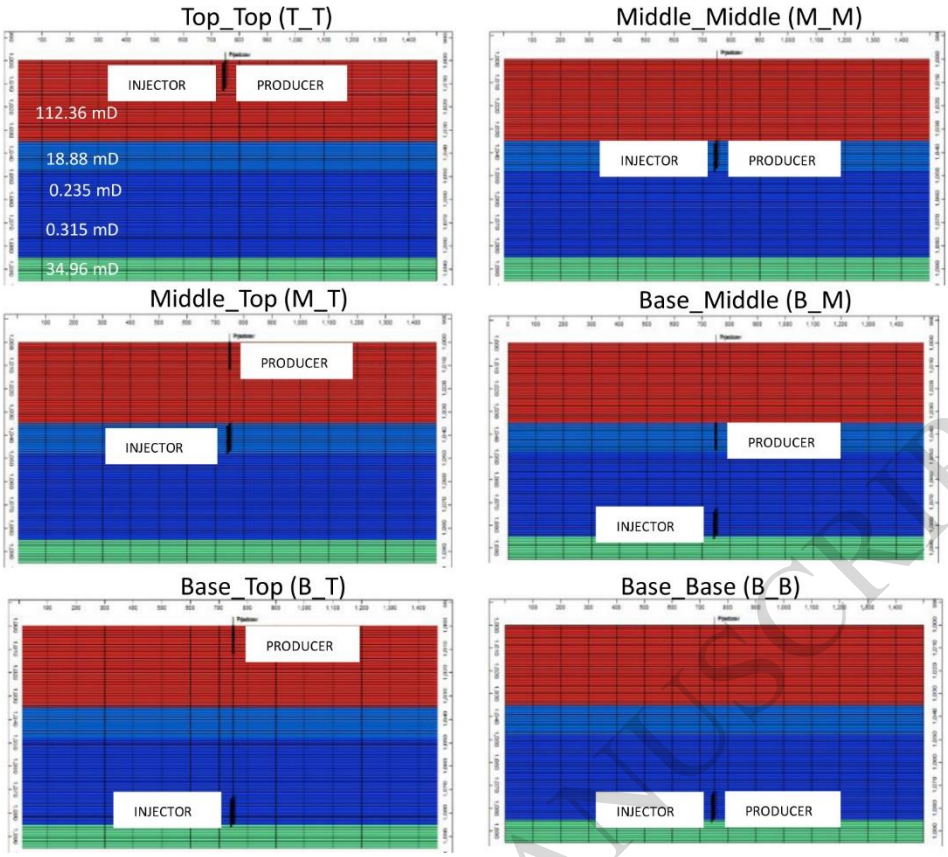

Figure 3

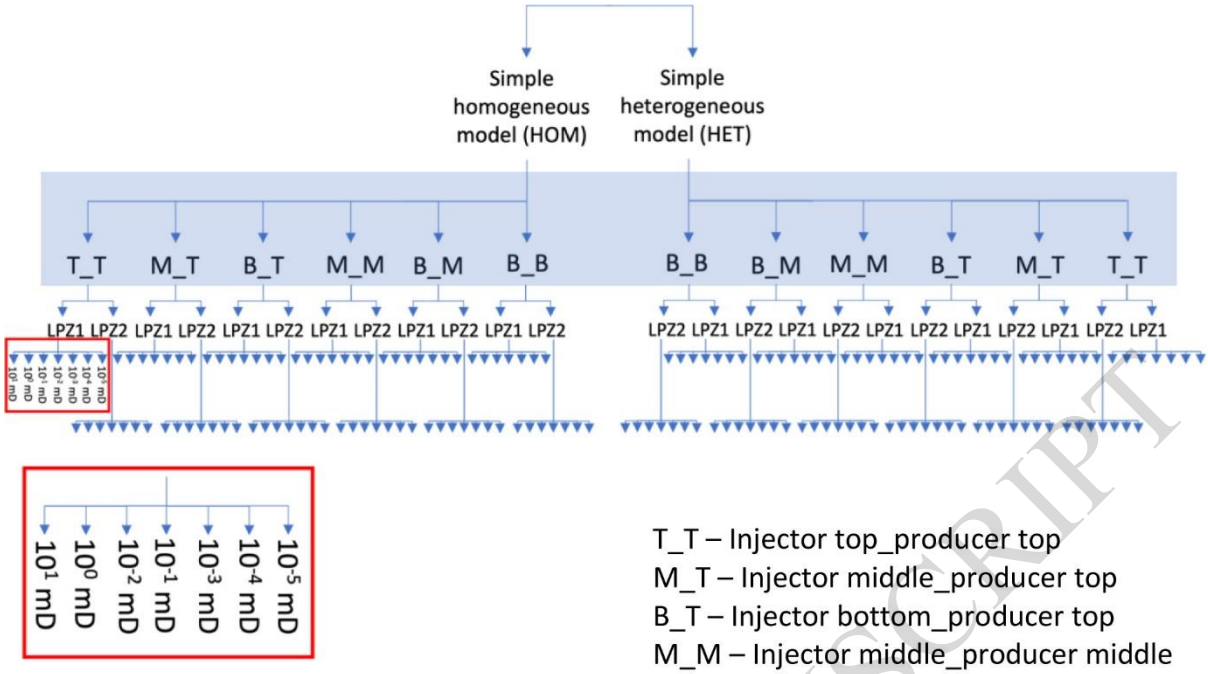

T_T – Injector top_producer top
M_T – Injector middle_producer top
B_T – Injector bottom_producer top
M_M – Injector middle_producer middle
B_M – Injector bottom_producer middle
B_B – Injector bottom_producer bottom

Figure 4

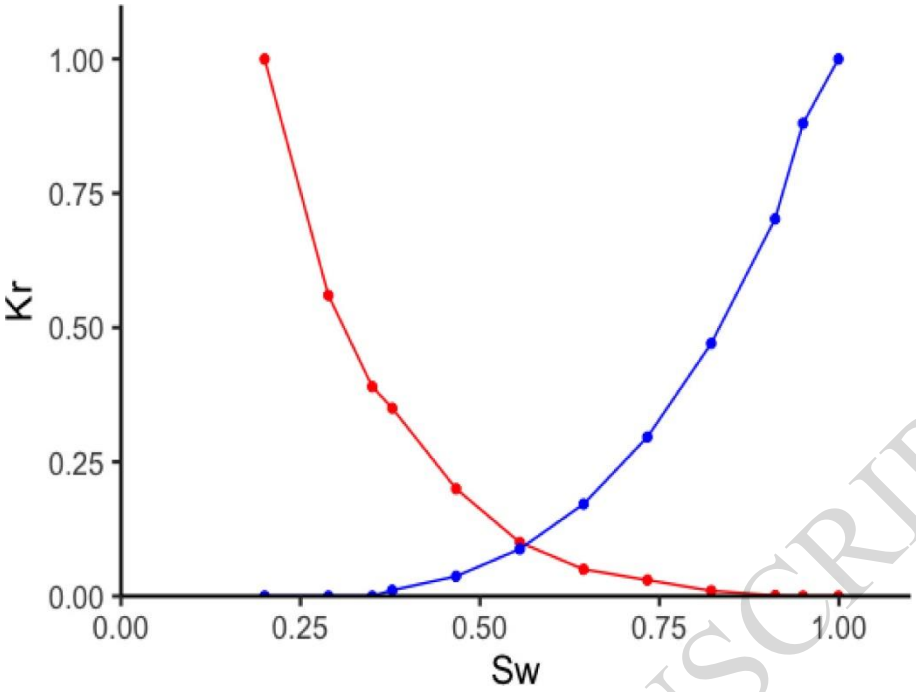

Figure 5

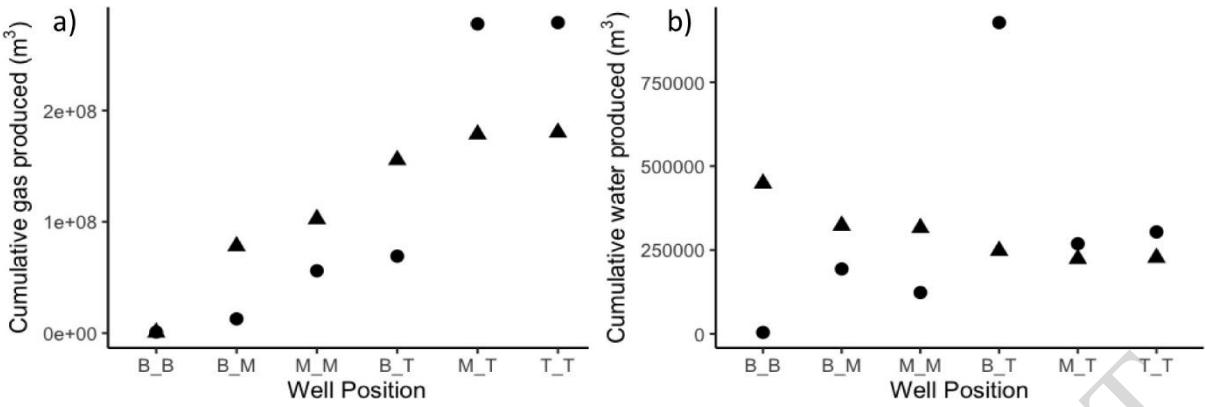

Figure 6

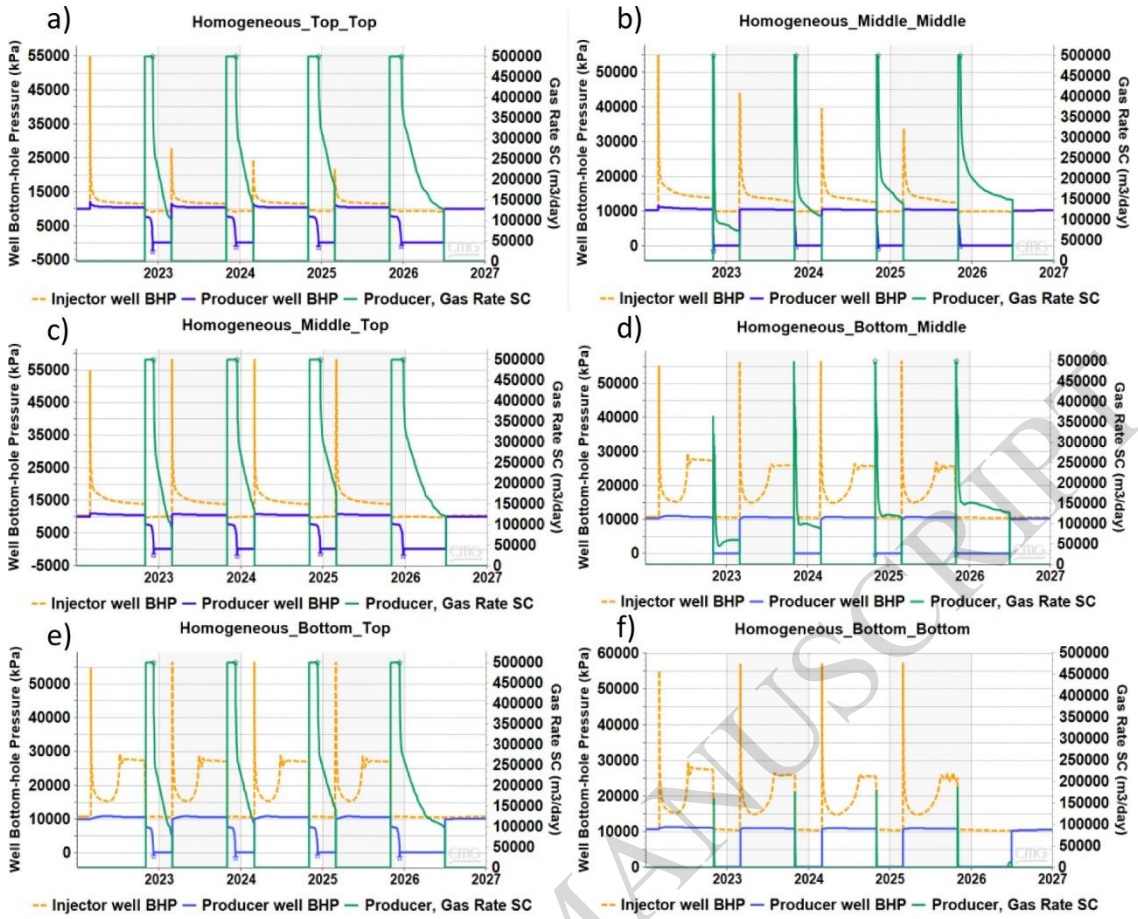

Figure 7

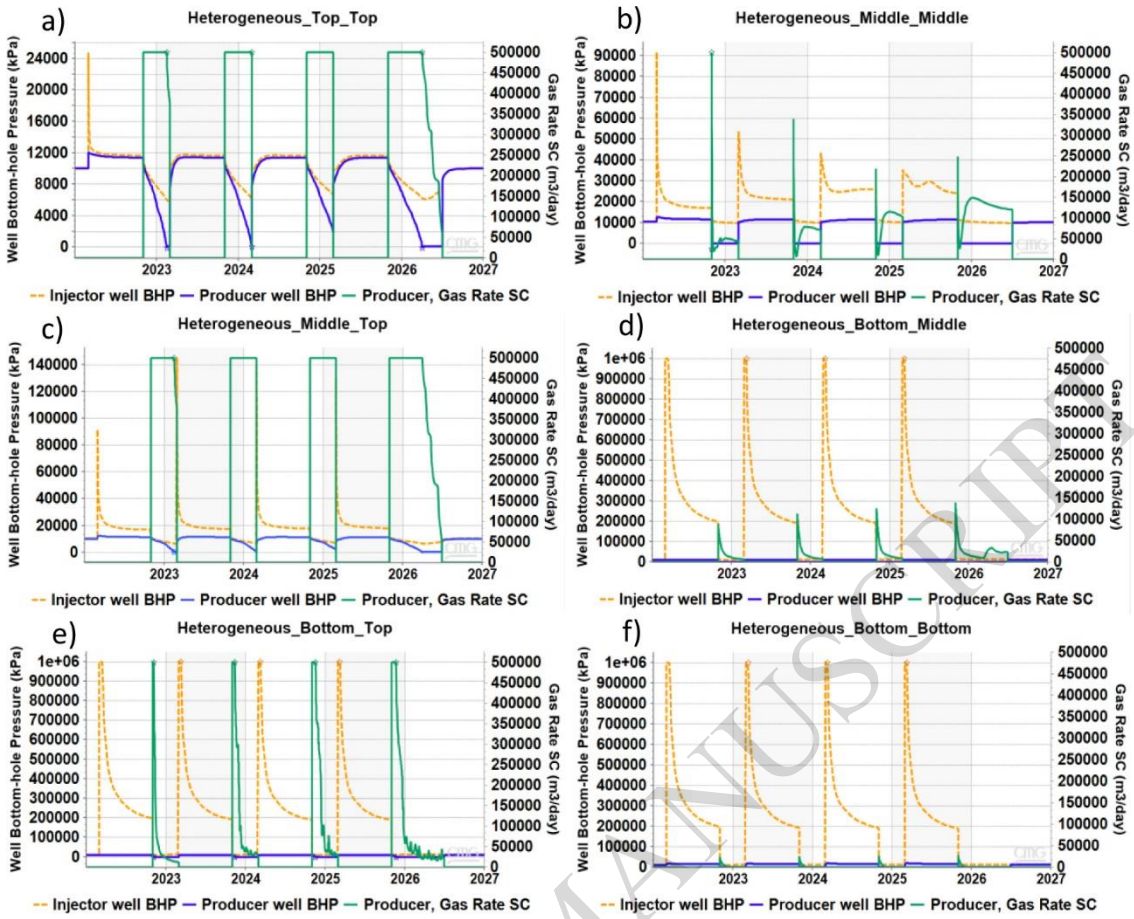

Figure 8

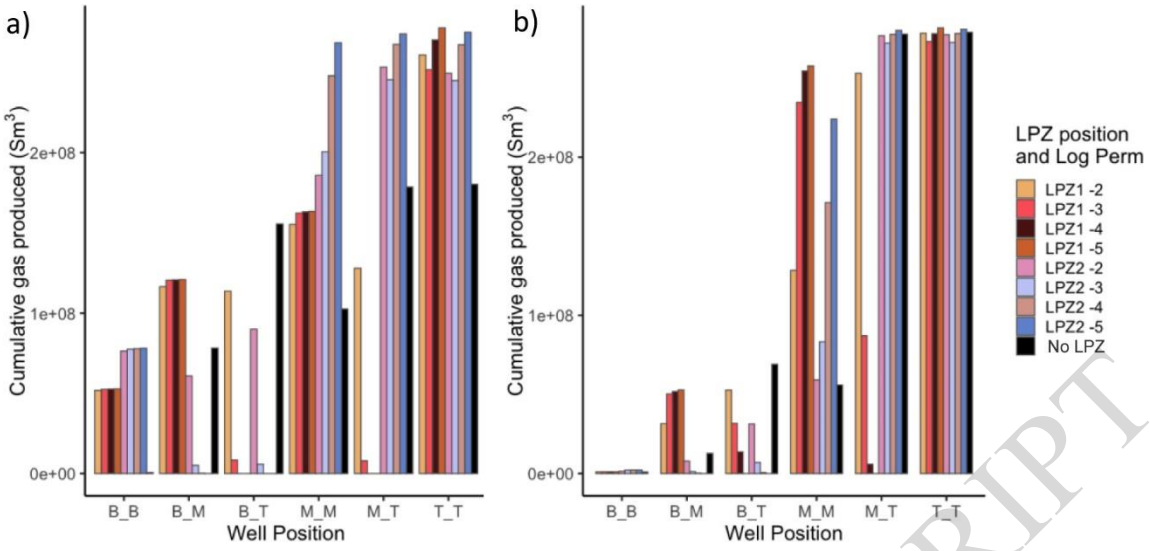

Figure 9

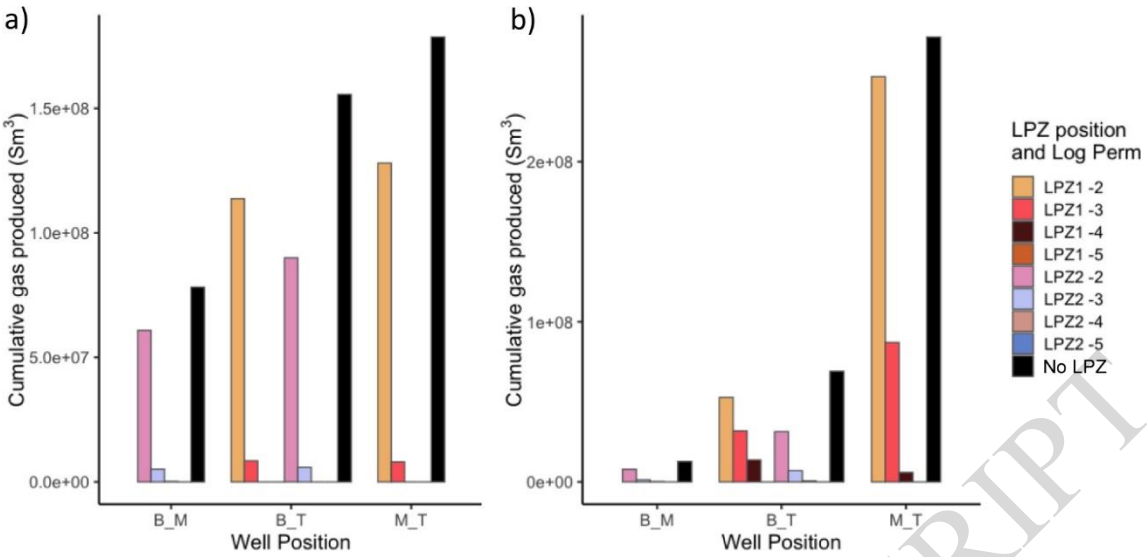

Figure 10

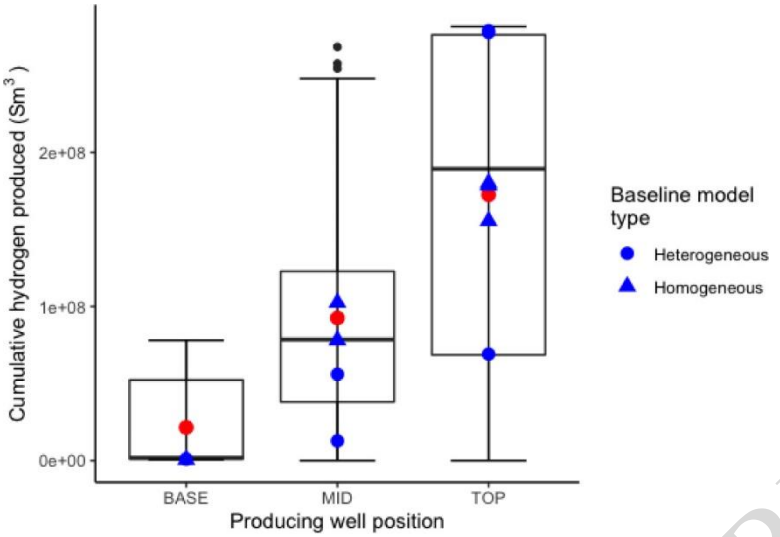

Figure 11

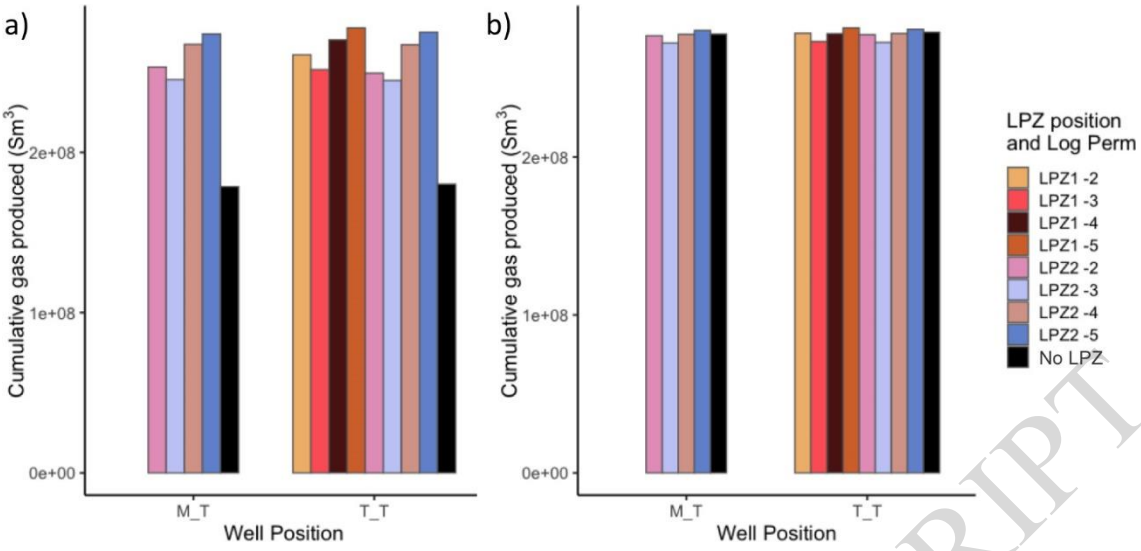

Figure 12

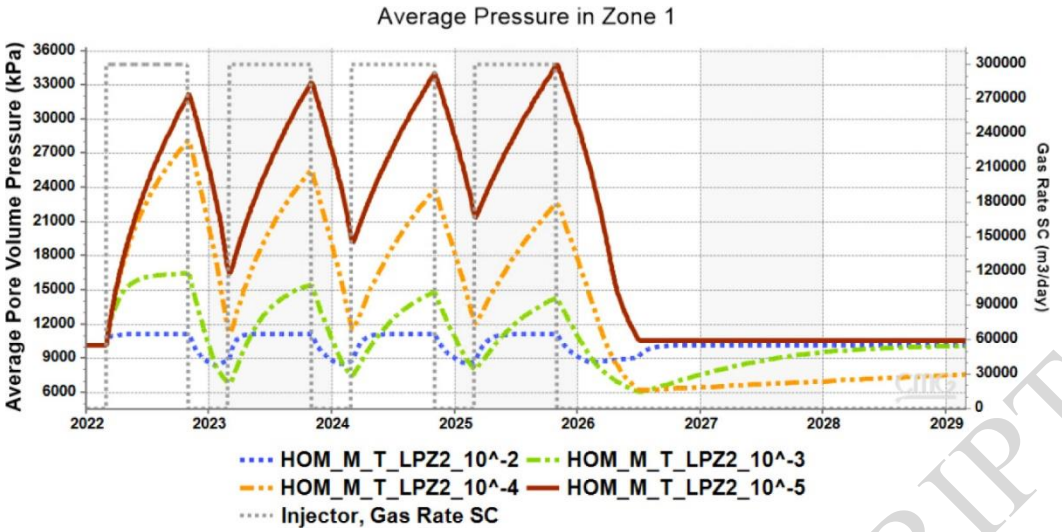

Figure 13

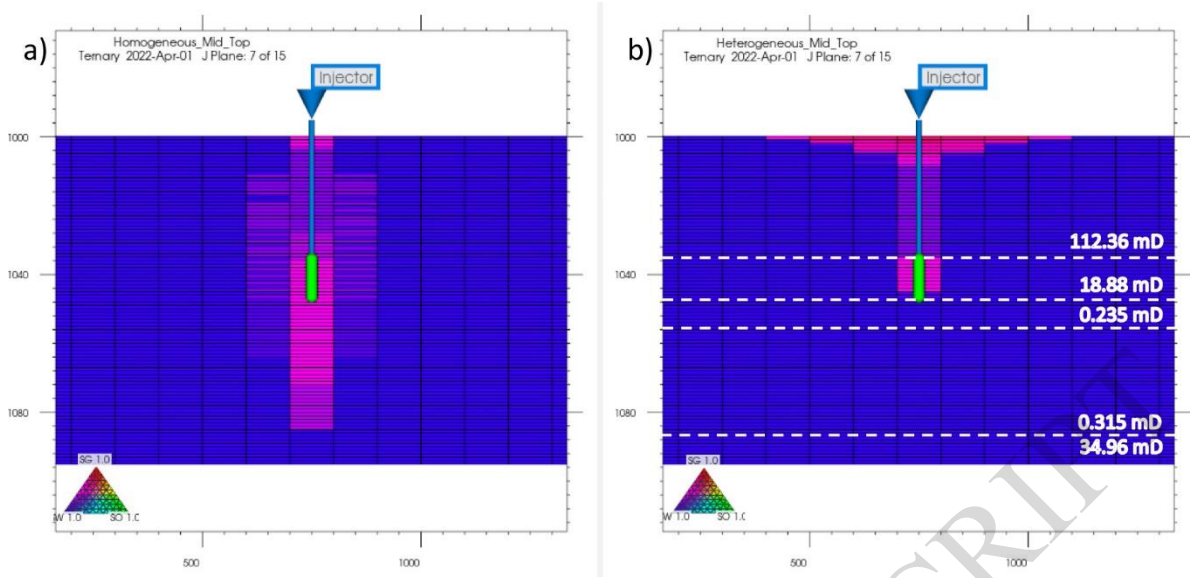

Figure 14

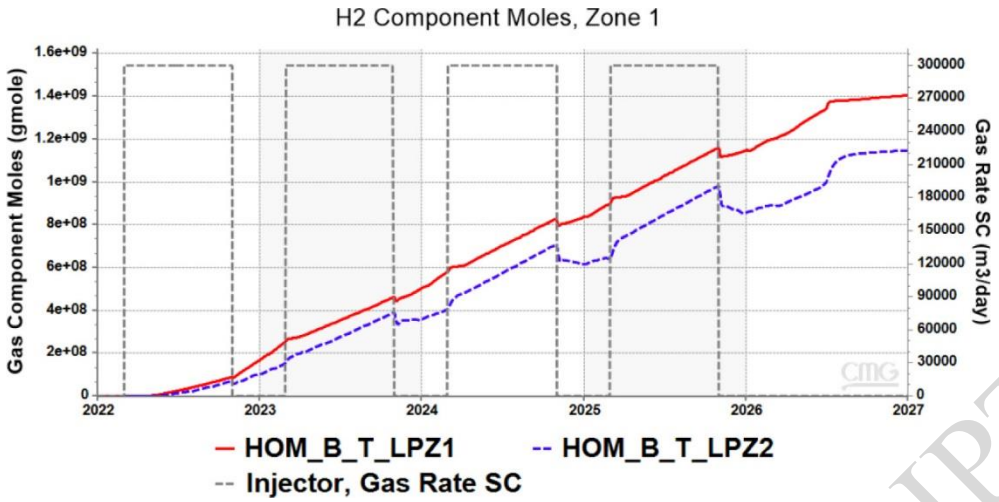

Figure 15

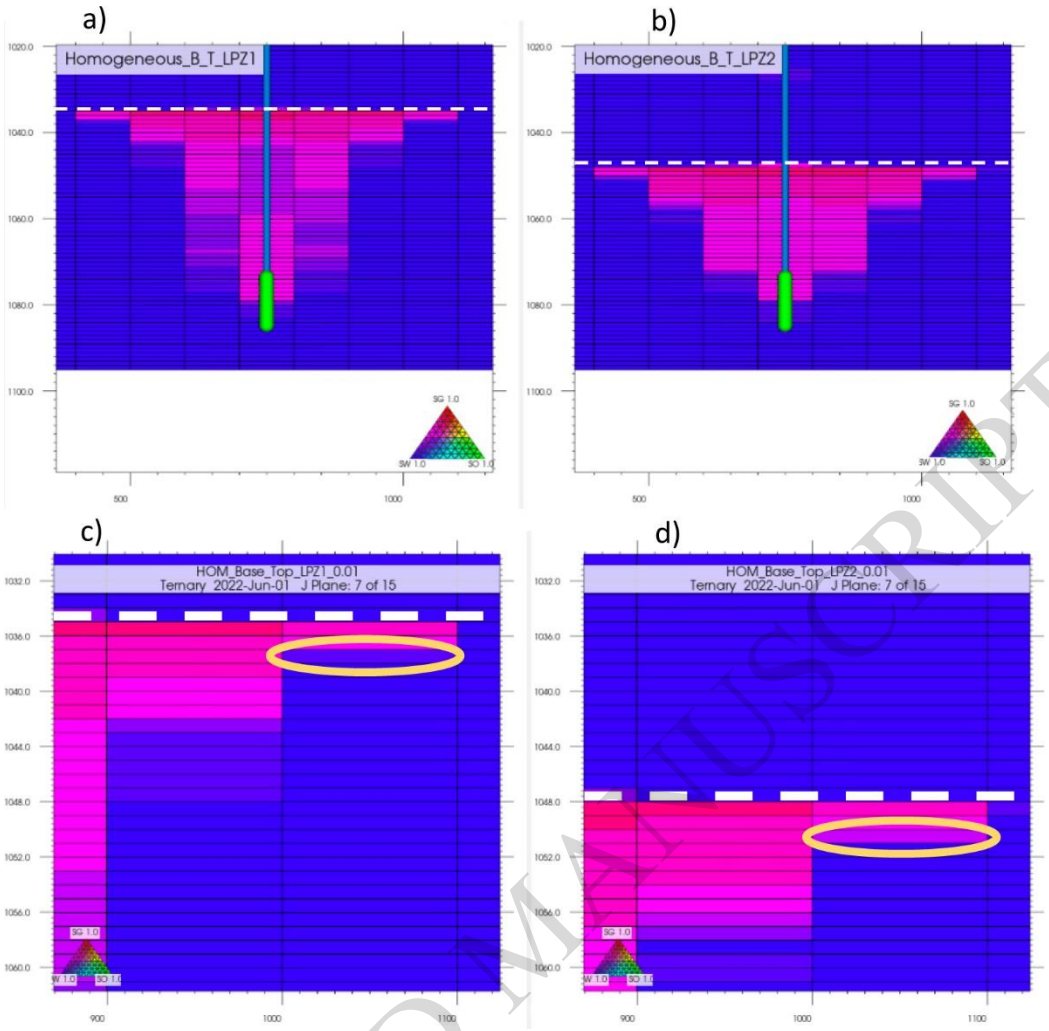

Figure 16